
***DIFFUSIVE DYNAMICS OF INTERACTING
PARTICLES IN EQUILIBRIUM AND UNDER
HYDRODYNAMIC SEDIMENTATION***

Jukka M. Lahtinen



*Laboratory of Physics
Helsinki University of Technology*

*Fysiikan laboratorio
Teknillinen korkeakoulu*

DISSERTATION 115 (2002)

Diffusive dynamics of interacting particles in equilibrium and under hydrodynamic sedimentation

Jukka M. Lahtinen

*Laboratory of Physics
Helsinki University of Technology
Espoo, Finland*

Dissertation for the degree of Doctor of Science in Technology to be presented with due permission of the Department of Engineering Physics and Mathematics, Helsinki University of Technology for public examination and debate in Auditorium K at Helsinki University of Technology (Espoo, Finland) on the 23rd of August, 2002, at 12 o'clock noon.

Dissertations of Laboratory of Physics, Helsinki University of Technology
ISSN 1455-1802

Dissertation 115 (2002):

Jukka M. Lahtinen: Diffusive dynamics of interacting particles in equilibrium and under hydrodynamic sedimentation

ISBN 951-22-6057-3 (print)

ISBN 951-22-6058-1 (electronic)

OTAMEDIA OY
ESPOO 2002

Abstract

Diffusive motion of particles plays an important role in many phenomena in surface physics, for example in chemical reactions, surface growth, and spreading. Diffusive motion can be observed in many different systems. In this thesis we study diffusion and dynamics in two fundamentally different kinds of systems: (i) in Brownian surface systems, and (ii) in a non-Brownian system of sedimenting particles with full hydrodynamic interactions. The quantities of central importance are the diffusion coefficients and the related correlation functions. In the sedimentation system we also discuss the behavior of the velocity fluctuations which has attracted a lot of attention recently.

First we study the system of spherical Brownian particles on a smooth surface. We find that while the tracer diffusion coefficient is a decreasing function of density, as expected, the collective diffusion coefficient strongly increases with increasing density. This behavior is completely dictated by the isothermal compressibility, since the center of mass mobility is independent of density in this system. Then we consider the influence of a periodic surface potential and the relation of the continuum model to the lattice gas model. It turns out that the lattice gas model approximates well the dynamics of the continuum model except at the limit when coverage approaches unity. Next we present the corresponding results in a system of rodlike molecules. For the rodlike molecules the normalized tracer diffusion coefficient is found to behave exactly as the tracer diffusion coefficient of the single spheres, while the collective diffusion coefficient is strongly enhanced.

In the system of sedimenting non-Brownian particles we find that the average sedimentation velocity of spherical particles decreases monotonically as a function of density but deviates from the phenomenological Richardson-Zaki law at the lowest densities. However, the average sedimentation velocity of spheroids displays non-monotonic behavior as a function of density. The maximum at the intermediate densities is attributed to a change in the orientational distribution of the spheroids. Finally, we study velocity fluctuations and diffusion coefficients in a system of sedimenting spherical particles confined between two parallel vertical walls. We find that the velocity fluctuations in the direction parallel to gravity grow linearly with system size, while the velocity fluctuations in the horizontal directions saturate. Also the tracer diffusion coefficient, which is closely related to the velocity fluctuations, demonstrates similar behavior.

Preface

The work reported in this thesis has been carried out in Helsinki Institute of Physics and Laboratory of Physics at Helsinki University of Technology during the years 1998-2002.

I would like to thank my advisor Prof. Tapio Ala-Nissilä for his guidance and support that have made this work possible. Without his enthusiasm it would have taken me far longer to complete this thesis.

I also wish to thank all the coauthors of the publications included in this thesis, especially Esa Kuusela, Doc. Tuomo Hjelt and Prof. Zdenek Chvoj. Furthermore, I wish to thank the pre-examiners Prof. Riccardo Ferrando and Prof. Liao Chen.

I have had the pleasure to work in an excellent group with many fine people and therefore it is in order to extend my thanks to all the members of the statistical materials physics group who have contributed to the inspiring atmosphere of the group.

The computational resources provided by the Center for Scientific Computing and the financial support of the Väisälä and Wihuri foundations are also gratefully acknowledged.

Finally, I would like to express my warmest thanks to my wife Anne, who has given me her full support during these years.

Espoo, July 2002

Jukka M. Lahtinen

List of Publications

This thesis consists of an overview and the following publications in the field of theoretical condensed matter physics:

- I. J. M. Lahtinen, T. Hjelt and T. Ala-Nissila, "Diffusive spreading of rodlike molecules on surfaces", *Surface Science*, **454-456**, 598 (2000).
- II. J. M. Lahtinen, T. Hjelt, T. Ala-Nissila, and Z. Chvoj, "Diffusion of hard disks and rodlike molecules on surfaces", *Physical Review E*, **64**, 021204 (2001).
- III. T. Hjelt, E. Kuusela, J. M. Lahtinen, T. Ala-Nissila, I. Vattulainen, and S. C. Ying, "Memory Effects and Memory Functions in Surface Diffusion", in "Collective Diffusion on Surfaces: Correlation Effects and Adatom Interactions", ed. by M. C. Tringides and Z. Chvoj, pp. 47-57, Kluwer (2001).
- IV. J. M. Lahtinen, M. Mašín, T. Laurila, T. Ala-Nissila, and Z. Chvoj, "Many-particle diffusion in continuum: Influence of a periodic surface potential", *Journal of Chemical Physics*, **116**, 7666 (2002).
- V. E. Kuusela, J. M. Lahtinen, and T. Ala-Nissila, "Orientational ordering of spheroids under finite Reynolds number sedimentation", Submitted to *Physical Review Letters* (2002).

The author has been actively involved in all stages of the work reported in this thesis. He has participated in planning the research work, and has developed the Molecular Dynamics and Monte Carlo simulation programs used in Publications I, II, and IV. The author has carried out all the simulations reported in Publications I, II and IV and some of the simulations reported in Publications III and V. He has also been responsible for the analysis of the results. The author has written publications I, II, IV, and has contributed actively to the writing of publications III and V. Finally, the author has been involved in the work reported in Ref. [1], and results obtained by him are also presented in this thesis.



Contents

| | |
|--|------------|
| Abstract | i |
| Preface | ii |
| List of Publications | iii |
| 1 Introduction | 1 |
| 2 Equilibrium diffusion on surfaces | 5 |
| 2.1 Brownian motion | 5 |
| 2.2 Tracer diffusion | 8 |
| 2.3 Collective diffusion | 9 |
| 2.4 Angular diffusion | 12 |
| 2.5 Generalized Langevin equation and memory functions | 12 |
| 2.6 Microscopic theories for a single particle | 13 |
| 2.7 Many-particle case | 15 |
| 2.7.1 Lattice gas model | 15 |
| 2.7.2 Continuum case | 17 |
| 3 Sedimentation of non-Brownian particles | 21 |
| 3.1 Sedimentation dynamics | 21 |
| 3.2 The model | 26 |

| | | |
|----------|---|-----------|
| 4 | Methods | 29 |
| 4.1 | Molecular Dynamics | 29 |
| 4.2 | Monte Carlo methods | 31 |
| 4.3 | Computation of the diffusion coefficients | 34 |
| 4.3.1 | The memory expansion method | 34 |
| 4.3.2 | The Boltzmann-Matano method | 37 |
| 4.4 | Computation of the thermodynamic factor | 38 |
| 5 | Results | 41 |
| 5.1 | Continuum limit | 41 |
| 5.2 | The influence of an external potential | 43 |
| 5.3 | The velocity autocorrelation functions in the surface systems | 52 |
| 5.4 | Diffusion of rodlike molecules | 53 |
| 5.5 | Sedimentation of non-colloidal particles | 59 |
| 5.5.1 | Three dimensional system | 59 |
| 5.5.2 | System confined between walls | 62 |
| 5.6 | Velocity autocorrelation function in the sedimentation system | 65 |
| 6 | Summary and discussion | 69 |

Chapter 1

Introduction

The concept of Brownian motion has been known for almost two centuries now. It is a manifestation of the continuous microscopic energy fluctuations in a system in thermal equilibrium. It was first observed by the botanist Robert Brown in 1828. He noted that pollen particles of different plants in water perform an uninterrupted random motion. Similar behavior can be observed for example in a system of particles adsorbed on a surface or in a colloidal system in which very small but macroscopic particles are immersed in a liquid. From the point of view of the diffusing particle this random motion is caused by the particle's coupling to the thermal fluctuations of the substrate, or, in the case of a colloidal particle, its collisions with the very large number of atomic size fluid particles. Over time this random motion causes a particle in the system to travel, or diffuse, far away from its original position. As a result for example a droplet of liquid or adsorbed gas on a surface spontaneously spreads and eventually the molecules evenly cover the whole surface.

This kind of diffusive motion of particles plays an important role in many phenomena in surface physics, for example in chemical reactions taking place on surfaces where the molecules diffuse around the surface before meeting their reaction partners. Also in the process of growing thin surface films where atoms are deposited on the surface they diffuse around to eventually form the film. In modern nanotechnology with the ever decreasing size of the structures, diffusion becomes a relevant phenomenon.

The mass of most adsorbed atoms and molecules is so large that their motion can be considered as classical. Perhaps the only notable exception is the

diffusion of a hydrogen atom, where it can be shown that quantum effects may play an important role [2].

The dynamics of these systems has been studied mostly in a system containing only one particle and not much is known about the many-particle dynamics. Taking into account realistic substrate dynamics, or a finite density of particles the interactions among the particles lead to complicated many-body effects which can be solved analytically only in special cases [2–4]. Under such circumstances computer simulations offer a way to make controlled experiments and to gain some understanding of the behavior of the system.

Brownian motion like behavior can also be observed in a non-colloidal suspension of particles sedimenting in a fluid. Non-colloidal particles are large enough such that the random collisions with the fluid molecules no longer play a role and the motion of the particles can be regarded as deterministic.

There are two slightly different ways of realizing the sedimentation process experimentally. We show them in Fig. 1.1. The first one is the batch sedimentation system where the sedimenting particles are released from the supernatant on the surface of the liquid and are then allowed to sediment to the bottom of the container. Alternatively, the sedimenting particles can be first evenly mixed into the liquid and then allowed to sediment freely. In this fluidized bed experimental setup, shown schematically in Fig. 1.1 (b), the particles never reach the bottom of the container because the liquid is kept in an upward motion such that on average the particles do not fall down.

A single particle sedimenting in a fluid goes straight down to the bottom of the container. Two particles form a pair, whose velocity can also have a horizontal component. Three or more particles form a many-body system whose dynamics becomes chaotic. The particles influence their mutual trajectories through the motion of the fluid. Due to backflow of the fluid induced by the settling particles even the average settling velocity becomes a non-trivial matter. If we look at the motion of the particles in a frame of reference which moves with the average settling velocity of the particles, the dynamics of the system is in many ways similar to the random Brownian motion even though there is nothing that causes thermal randomness in the system.

In this thesis we study the diffusive dynamics in the above described strongly interacting many-body systems. Depending on the details of the system dif-

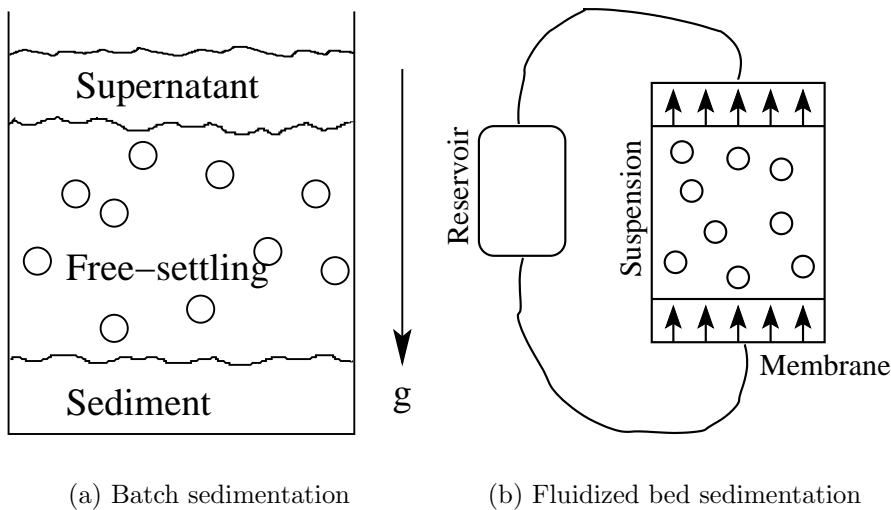


Figure 1.1: Experimental setups for sedimentation.

ferent phases such as a liquid or a crystal phase may exist. In this thesis we concentrate only on the liquid-like phase and in general do not concern ourselves with the phase transitions or possible other phases in the systems under study. The central quantities of interest are the diffusion coefficients and the related velocity autocorrelation functions and their memory functions, velocity fluctuations, and the static structure factor. In particular we concentrate on the density dependence of these quantities and the underlying mechanisms that give rise to the observed behavior.

In this overview we will first in Chapter 2 define and discuss some basic concepts of diffusive motion. The meaning of these concepts will be illustrated through the behavior of a single Brownian particle. In the second Chapter we also introduce the lattice gas and continuum models of surface diffusion giving a short review of the relevant theoretical results available in the literature. The sedimentation system is introduced in Chapter 3. This Chapter begins with an introduction to concepts specific to the sedimentation system. In the second half of the Chapter some details of the actual model used are given. Chapter 4 introduces the methods and techniques used in this thesis. This Chapter begins with an introduction of the simulation methods, namely the Molecular Dynamics and the Monte Carlo methods. Then we go on to discuss methods for computing the diffusion coefficients from the simulations. The memory expansion method is a use-

ful tool for computing both the tracer and collective diffusion coefficients and the Boltzmann-Matano method is an efficient and widely used method in experimental physics to study the collective diffusion coefficient and can be also utilized in simulations. Chapter 5 gives an overview of the most important results obtained in this thesis. First the behavior of the diffusion coefficients in a smooth surface system of single spheres is discussed. We find that while the tracer diffusion coefficient is a decreasing function of density, as expected, the collective diffusion coefficient strongly increases with increasing density. This behavior is completely dictated by the isothermal compressibility, since the center of mass mobility is independent of density in this system. Then we consider the influence of a periodic surface potential and the relation of the continuum model to the lattice gas model. It turns out that the lattice gas model approximates well the dynamics of the continuum model except at the limit where coverage approaches unity. Next we present the corresponding results in a system of rodlike molecules. For the rodlike molecules the normalized tracer diffusion coefficient is found to behave exactly as the tracer diffusion coefficient of single spheres, that is the rod length does not appear to have any effect. Then we go on by discussing the temporal decay properties of the velocity autocorrelation function in all of the different systems studied. Finally, we give an overview of our sedimentation system results including the work reported in Ref. [1]. In the sedimentation system we find that the average sedimentation velocity of spherical particles decreases monotonically as a function of density but deviates from the phenomenological Richardson-Zaki law at the lowest densities. However, the average sedimentation velocity of spheroids displays non-monotonic behavior as a function of density. The maximum at the intermediate densities is attributed to a change in the orientational distribution of the spheroids. Last, we study velocity fluctuations and diffusion coefficients in a system of sedimenting spherical particles confined between two parallel vertical walls. We find that the velocity fluctuations in the direction parallel to gravity grow linearly with system size, while the velocity fluctuations in the horizontal directions saturate. The thesis ends in a summary and discussion in Chapter 6.

Chapter 2

Equilibrium diffusion on surfaces

2.1 Brownian motion

Let us first consider the most classical example of diffusion: the Brownian motion. A particle suspended in a liquid undergoes random motion caused by the collisions between the particle and the surrounding liquid molecules. The particle has no preferred direction and at any instant in time it is not possible to predict in what direction the particle is moving.

Consider a single isolated Brownian particle. If we assume that the motion of the Brownian particle is essentially decoupled from the motion of the fluid particles, that is the motion of the liquid adapts instantaneously to the motion of the Brownian particle, we can write down the equation of motion of such a particle as

$$m \frac{d}{dt} \vec{v}(t) = -\eta m \vec{v}(t) + \vec{F}(t), \quad (2.1.1)$$

where m is the mass of the particle, $\vec{v}(t)$ its velocity at time t , η is the friction coefficient and $\vec{F}(t)$ is a random force acting on the particle. This equation of motion is called the Langevin equation. The effect of the surrounding liquid is on the right hand side of the equation and it is divided into two terms. The first term represents the systematic drag that the liquid puts on the particle. The second term represents the random collisions of the

liquid particles with the Brownian particle. The random force is assumed to be white noise and uncorrelated with the motion of the Brownian particle, that is

$$\langle \vec{F}(t) \rangle = 0, \quad \text{and} \quad \langle \vec{F}(t) \cdot \vec{v}(t) \rangle = 0. \quad (2.1.2)$$

It is also assumed that the correlation time of the random force is infinitely short

$$\langle \vec{F}(t) \cdot \vec{F}(t') \rangle = 2\pi F_0 \delta(t - t'). \quad (2.1.3)$$

In here and in the following discussion the brackets $\langle \rangle$ denote an ensemble average.

The two terms on the right-hand side of Eq. (2.1.1) are not independent. We can show that there is a connection between the friction coefficient η and the constant F_0 . To this end we first write the solution to (2.1.1) as

$$m \vec{v}(t) = m \vec{v}(0) \exp(-\eta t) + \exp(-\eta t) \int_0^t \exp(\eta s) \vec{F}(s) ds. \quad (2.1.4)$$

If we square this and take the mean we find, using (2.1.2) and (2.1.3), that

$$\begin{aligned} m^2 \langle |\vec{v}(t)|^2 \rangle &= m^2 \langle |\vec{v}(0)|^2 \rangle \exp(-2\eta t) + \\ &\exp(-2\eta t) \int_0^t \int_0^t \exp[\eta(s + s')] 2\pi F_0 \delta(s - s') ds' ds \\ &= m^2 \langle |\vec{v}(0)|^2 \rangle \exp(-2\eta t) + \frac{\pi F_0}{\eta} [1 - \exp(-2\eta t)]. \end{aligned} \quad (2.1.5)$$

Next we consider this solution in the long time limit when the Brownian particle has completely equilibrated regardless of the initial conditions, that is we take the limit $t \rightarrow \infty$. From the equipartition theorem we know that

$$\langle |\vec{v}(\infty)|^2 \rangle = \frac{d k_B T}{m}, \quad (2.1.6)$$

where d is the dimension of the system, T the temperature and k_B Boltzmann constant. From this it follows that

$$F_0 = \frac{d \eta m k_B T}{\pi}. \quad (2.1.7)$$

This links the fluctuations which are of microscopic origin to the macroscopically observable dissipation in the Langevin equation (2.1.1). This is an example of the fluctuation-dissipation theorem [5].

2.1 Brownian motion

Let us next consider the behavior of the Brownian particle in the long time limit, and specifically consider the mean square displacement $\langle |\vec{r}(t) - \vec{r}(0)|^2 \rangle$. Without any loss of generality let us assume that the particle is initially at the origin $\vec{r}(0) = 0$ to simplify things. If we multiply the Langevin equation (2.1.1) by $\vec{r}(t)$ and use the results

$$\vec{r} \cdot \vec{v} = \vec{r} \cdot \dot{\vec{r}} = \frac{1}{2} \frac{d}{dt} r^2, \quad (2.1.8)$$

$$\vec{r} \cdot \dot{\vec{v}} = \vec{r} \cdot \ddot{\vec{r}} = \frac{1}{2} \frac{d^2}{dt^2} r^2 - v^2, \quad (2.1.9)$$

we find that

$$\frac{1}{2} m \frac{d^2}{dt^2} |\vec{r}(t)|^2 + \frac{1}{2} \eta m \frac{d}{dt} |\vec{r}(t)|^2 = m |\vec{v}(t)|^2 + \vec{r}(t) \cdot \vec{F}(t). \quad (2.1.10)$$

Taking the statistical mean and again using the equipartition theorem this yields

$$\frac{d^2}{dt^2} \langle |\vec{r}(t)|^2 \rangle + \eta \frac{d}{dt} \langle |\vec{r}(t)|^2 \rangle = \frac{2d k_B T}{m}. \quad (2.1.11)$$

This is an ordinary differential equation for the mean square displacement which we can easily solve. Using the initial conditions

$$\langle |\vec{r}(0)|^2 \rangle = 0, \quad (2.1.12)$$

and

$$\frac{d}{dt} \langle |\vec{r}(0)|^2 \rangle = 2 \langle \vec{r}(0) \cdot \vec{v}(0) \rangle = 0, \quad (2.1.13)$$

the solution becomes

$$\langle |\vec{r}(t)|^2 \rangle = \left(\frac{2d k_B T}{\eta m} \right) \left[t - \frac{1}{\eta} + \frac{1}{\eta} \exp(-\eta t) \right]. \quad (2.1.14)$$

In the long time limit when $\eta t \gg 1$ we see that the mean square displacement grows linearly in time

$$\langle |\vec{r}(t)|^2 \rangle \propto \left(\frac{2d k_B T}{\eta m} \right) t. \quad (2.1.15)$$

This is the hallmark of diffusive motion, in contrast to $\langle |\vec{r}(t)|^2 \rangle \propto t^2$ for ballistic motion.

2.2 Tracer diffusion

For characterizing the diffusive motion there exists several distinct diffusion coefficients. In this thesis we concentrate on the tracer diffusion coefficient D_T , the collective diffusion coefficient D_C , and the angular diffusion coefficient D_R .

Let us first define the tracer diffusion coefficient. As noted above the mean square displacement of a Brownian particle depends linearly on time. This is a general property of diffusive motion and it is precisely this property that is used for defining D_T . Consider a single particle i in a system of N particles. The tracer diffusion coefficient is defined as

$$D_T = \lim_{t \rightarrow \infty} \frac{1}{2dt} \langle |\vec{r}_i(t) - \vec{r}_i(0)|^2 \rangle. \quad (2.2.1)$$

That is it is the slope of the mean square displacement of a single particle i at the long time limit. In the case of a single isolated Brownian particle we can see from Eq. (2.1.15) that

$$D_T = \frac{k_B T}{m \eta}, \quad (2.2.2)$$

which is inversely proportional to the friction coefficient η .

A quantity closely related to the tracer diffusion coefficient is the velocity autocorrelation function

$$\phi(t) = \langle \vec{v}_i(t) \cdot \vec{v}_i(0) \rangle, \quad (2.2.3)$$

where $\vec{v}_i(t)$ is the velocity of a single particle i at time t . To see the connection between this and the tracer diffusion coefficient we again make the choice $\vec{r}(0) = 0$ and thus have

$$\begin{aligned} \langle |\vec{r}_i(t)|^2 \rangle &= \left\langle \left| \int_0^t \vec{v}_i(t') dt' \right|^2 \right\rangle = \left\langle \int_0^t \vec{v}_i(t'') dt'' \cdot \int_0^t \vec{v}_i(t') dt' \right\rangle \\ &= \int_0^t \int_0^t \langle \vec{v}_i(t') \cdot \vec{v}_i(t'') \rangle dt'' dt'. \end{aligned} \quad (2.2.4)$$

With the substitution $s = t' - t''$ the last integral yields

$$\langle |\vec{r}_i(t)|^2 \rangle = 2 \int_0^t (t - s) \langle \vec{v}_i(0) \cdot \vec{v}_i(s) \rangle ds. \quad (2.2.5)$$

2.3 Collective diffusion

Then we just plug this into the definition of the tracer diffusion coefficient (2.2.1)

$$D_T = \frac{1}{d} \lim_{t \rightarrow \infty} \int_0^t \frac{t-s}{t} \phi(s) ds = \frac{1}{d} \int_0^\infty \phi(s) ds, \quad (2.2.6)$$

since eventually at long times $\vec{v}_i(t)$ becomes uncorrelated with $\vec{v}_i(0)$, the velocity autocorrelation function goes to zero and thus s in the integrand remains finite. An expression such as Eq. (2.2.6), where a transport coefficient is described in terms of a time-correlation function of some dynamic variable is known as a Green-Kubo equation [6].

2.3 Collective diffusion

So far we have looked at the diffusion of a single particle. As already mentioned above there is also another diffusion coefficient, the collective diffusion coefficient D_C . In order to define it and illustrate its meaning let us first take the hydrodynamic approach. In the hydrodynamic regime we are dealing with length and time scales much larger than the microscopic ones.

The first ingredient we need is the conservation of particles in the system. This can be expressed mathematically by the continuity equation

$$\frac{\partial \rho}{\partial t} + \nabla \cdot \vec{j} = 0. \quad (2.3.1)$$

Here ρ is the density of the particles and \vec{j} is the particle current density. Secondly a connection between these two is taken as the phenomenological Fick's first law

$$\vec{j} = -D_C(\rho) \nabla \rho(\vec{r}, t), \quad (2.3.2)$$

which postulates that the particle current density is directly proportional to the density gradient. This is valid when $\nabla \rho(\vec{r}, t)$ is sufficiently small that terms having density gradients higher than second order can be neglected. This is a manifestation of linear response theory [5]. The coefficient of proportionality D_C is the collective diffusion coefficient. If we combine the above two expressions we obtain

$$\frac{\partial \rho}{\partial t} = \nabla \cdot D_C(\rho) \nabla \rho(\vec{r}, t), \quad (2.3.3)$$

which is called the diffusion equation. This is a non-linear partial differential equation and it is in general not analytically solvable. Therefore, it is often assumed that D_C is a constant or depends on the density only weakly and the diffusion equation is simplified into

$$\frac{\partial \rho}{\partial t} = D_C \nabla^2 \rho(\vec{r}, t), \quad (2.3.4)$$

which is often referred to as Fick's second law. This assumption, however, is not true for strongly interacting systems, as we will see later, and the collective diffusion coefficient depends strongly on the density.

It is worthwhile pointing out that the second assumption Eq. (2.3.2) is valid only when the system is close enough to equilibrium and the density gradients higher than second order can be neglected. This is not necessarily the case for example in the spreading of droplets. However, in some cases the spreading takes place under local quasi-equilibrium conditions and the linear response theory turns out to be at least approximately valid [7].

From the above discussion it should be clear that the collective diffusion coefficient deals with the collective motion of the particles. It measures the role of mass transport and the decay of density fluctuations in the system, whereas the tracer diffusion coefficient measures the role of diffusive motion of a single particle.

An alternative way of defining the collective diffusion coefficient is the Green-Kubo form. An expression analogous to the corresponding equation for the tracer diffusion, Eq. (2.2.6), reads for the collective diffusion as

$$D_C = \frac{\rho}{NS_0d} \int_0^\infty \langle \vec{J}(t) \cdot \vec{J}(0) \rangle dt, \quad (2.3.5)$$

where $\vec{J}(t)$ is the total flux given by

$$\vec{J}(t) = \sum_{i=1}^N \vec{v}_i(t). \quad (2.3.6)$$

The term S_0/ρ is the so-called thermodynamic factor, where S_0 is defined as the long wavelength limit of the static structure function. The static structure function is the zero time limit of the dynamic structure function defined as the Fourier transformation of the density-fluctuation autocorrelation function

$$S(\vec{r} - \vec{r}', t) \equiv \langle \delta\rho(\vec{r}', 0) \delta\rho(\vec{r}, t) \rangle, \quad (2.3.7)$$

2.3 Collective diffusion

where $\delta\rho \equiv \rho(\vec{r}, t) - \langle\rho\rangle$. Thus S_0 is given by

$$S_0 = \lim_{k \rightarrow 0} S(k, 0) = \lim_{k \rightarrow 0} \int e^{-i\vec{k} \cdot \vec{r}'} S(\vec{r}', 0) d\vec{r}'. \quad (2.3.8)$$

The thermodynamic factor is also related to the isothermal compressibility κ_T and to the particle number fluctuations through the relation [3]

$$S_0 = k_B T \rho^2 \kappa_T = \rho \frac{\langle(\delta N)^2\rangle}{\langle N\rangle}. \quad (2.3.9)$$

If there exists an equation of state for the system one can apply this relation to extract the thermodynamic factor.

Instead of using the definition (2.3.5) directly for the evaluation of the collective diffusion coefficient it is more convenient to write it in the form corresponding to Eq. (2.2.1) in the case of the tracer diffusion. In the case of collective diffusion this becomes

$$D_C = \frac{\rho}{S_0} D_{cm} = \frac{\rho}{S_0} \lim_{t \rightarrow \infty} \frac{1}{2Ntd} \langle |\vec{R}(t) - \vec{R}(0)|^2 \rangle. \quad (2.3.10)$$

Here $\vec{R}(t) = \sum_i \vec{r}_i(t)$ is N times the coordinate of the center of mass of the system and D_{cm} defined by the above expression is called the center of mass mobility. As can be seen from the definition, the center of mass mobility is the tracer diffusion coefficient of the center of mass of all particles.

The above definitions clearly illustrate the differences between the two diffusion coefficients. In addition to the dynamical part D_{cm} , the collective diffusion coefficient also contains the thermodynamic factor, which can display anomalous behavior *e.g.* in the vicinity of phase boundaries. Also, the dynamic part D_{cm} is a result of the motion of different particles at different times and we can therefore expect that the memory effects do not play such an important role in the collective diffusion as they do in the tracer diffusion.

A simple relation between the two diffusion coefficients would be very useful in practice since D_{cm} is generally much more difficult to compute numerically than D_T . In the limit $\rho \rightarrow 0$, that is when there is only one particle in the system, $D_C = D_{cm} = D_T$. However, at higher densities no such relation exists. There exists a rather popular approximate expression called the Darken equation [3]

$$D_C = \frac{\rho}{S_0} D_T. \quad (2.3.11)$$

This simply means approximating D_{cm} by D_T . This approximation is accurate only for non-interacting systems and becomes unreliable even for the most simple interacting systems [2].

2.4 Angular diffusion

For molecules which also have a rotational degree of freedom an angular (tracer) diffusion coefficient can be defined based on the rotational motion of the molecules. We do this in a way that is analogous to the definition of the tracer diffusion coefficient:

$$D_R = \lim_{t \rightarrow \infty} \frac{1}{2dt} \langle |\theta_i(t) - \theta_i(0)|^2 \rangle, \quad (2.4.1)$$

where $\theta_i(t)$ is the orientation of the molecule i at time t with respect to some fixed axis. It should be noted that $\theta_i(t)$ is not bounded in $[0, 2\pi]$. This is somewhat different from the usual rotational diffusion coefficient [8].

The angular diffusion coefficient D_R is useful for monitoring the rotational motion of the molecules. Especially if there is a phase transition in the system to an orientationally ordered nematic phase one would expect to see a drop in D_R . We have computed this quantity in the system of rodlike molecules in Section 5.4 to observe if any orientational ordering takes place.

2.5 Generalized Langevin equation and memory functions

The discussion of Section 2.1 was for a single particle diffusing in a system without any external potential. In a more general case we have a number of diffusing particles in the system which interact in some arbitrary way. In addition to interacting with each other the particles can also interact with the surface through some interaction potential. In such a system the Langevin equation (2.1.1) can be generalized to

$$m \frac{d}{dt} \vec{v}(t) = -\nabla V(\vec{r}(t)) - m \int_0^t M(t-t') \vec{v}(t') dt' + \vec{F}(t), \quad (2.5.1)$$

2.6 Microscopic theories for a single particle

where $V(\vec{r})$ is an external potential and the time dependent friction term $M(t)$ is called the memory function. It contains the memory of the earlier states of the system. This equation is called the Generalized Langevin Equation. In the Markovian limit $M(t) = \eta\delta(t)$ it reduces back to the same form as the Langevin equation (2.1.1) introduced above. Despite the fact that the Generalized Langevin Equation is often used as a phenomenological approach it can be derived from a microscopic Hamiltonian that incorporates the full degrees of freedom of the system using the Mori Projection Operator formalism [2, 4, 9–11].

The Generalized Langevin Equation can also be written for the velocity autocorrelation function $\phi(t)$ as [12]

$$\frac{d\phi(t)}{dt} = i\Omega_0\phi(t) - \int_0^t M_v(t-s)\phi(s)ds. \quad (2.5.2)$$

Here $i\Omega_0$ is the so called frequency variable which vanishes in continuum. Again in the Markovian limit the memory function $M_v(t)$ reduces to a delta function.

To determine $M_v(t)$ numerically we Fourier transform (2.5.2) and solve for the Fourier transform of the memory function

$$\tilde{M}_v(i\omega) + i\Omega_0 = \frac{1}{\tilde{\phi}(i\omega)} - i\omega. \quad (2.5.3)$$

In case the functions $\phi(t)$ and $M_v(t)$ are only known at discrete time steps this formula can be readily generalized using the discrete Fourier transformation. We discuss the behavior of the velocity autocorrelation function in different systems in Sections 5.3 and 5.6 and also compute the corresponding memory functions.

2.6 Microscopic theories for a single particle

In the low density limit when we have only one diffusing particle in the system both translational diffusion coefficients D_T and D_C introduced above are equal. The diffusion of a single particle in absence of an external surface potential was already discussed in Section 2.1. The simple result $D_C(0) = D_T(0) = k_B T/m\eta$ was obtained by solving the Langevin equation (2.1.1) explicitly.

In any realistic surface system the diffusing particle interacts with the surface through some interaction potential. Even in the case of a single diffusing particle the problem is inherently of many-body type due to the coupling of the particle to the substrate degrees of freedom. The resulting effect on the diffusing particle is described by the so-called adiabatic potential $V_A(\vec{r})$.

To define the adiabatic potential consider an interaction Hamiltonian of the form

$$\mathcal{H}_a = \mathcal{H}_s + \mathcal{H}_0 + \mathcal{H}_{int}, \quad (2.6.1)$$

where \mathcal{H}_s is the Hamiltonian for the substrate excitations and the adparticle Hamiltonian \mathcal{H}_0 is given by

$$\mathcal{H}_0 = \frac{\vec{p}^2}{2m} + V_s(\vec{r}), \quad (2.6.2)$$

where m is the mass of the diffusing adparticle and \vec{p} its momentum. The potential V_s is the rigid surface potential corresponding to an unperturbed surface. The remaining term \mathcal{H}_{int} consists of two parts. The first part is an adiabatic part which describes the local relaxation of the substrate caused by the adparticle. The second part is called the non-adiabatic part and it is due to the rapid thermal fluctuations of the substrate. The adiabatic potential $V_A(\vec{r})$ is defined as a sum of $V_s(\vec{r})$ and the adiabatic part of \mathcal{H}_{int} . Formally, we can write $\mathcal{H}_{int} = V(\vec{r}, \vec{R}_\ell)$ where $V(\vec{r}, \vec{R}_\ell)$ is a general interaction potential. The adiabatic potential $V_A(\vec{r})$ can be defined through

$$\exp\{-\beta[V_A(\vec{r}) - V_s(\vec{r})]\} \equiv \frac{1}{Z_s} \int \exp\{-\beta[\mathcal{H}_s + V(\vec{r}, \vec{R}_\ell)]\} \Pi_\ell d\vec{P}_\ell d\vec{R}_\ell, \quad (2.6.3)$$

where $\beta = 1/(k_B T)$, the capitalized coordinates refer to the substrate particles, $V(\vec{r}, \vec{R}_\ell) = \mathcal{H}_{int}$ and Z_s is a configuration integral

$$Z_s = \int \exp(-\beta\mathcal{H}_s) \Pi_\ell d\vec{P}_\ell d\vec{R}_\ell. \quad (2.6.4)$$

Thus the adiabatic potential contains all static information about the system. The minima of the adiabatic potential define the equilibrium adsorption sites and the diffusion barrier is the difference between the potential of the minima and the lowest saddle points.

The surface potentials studied in this thesis are considered to be adiabatic potentials. A model potential considered in Publication IV is the following separable one:

$$V_A(x, y) = V_0 \left[\cos\left(\frac{2\pi x}{a}\right) + \cos\left(\frac{2\pi y}{a}\right) \right], \quad (2.6.5)$$

2.7 Many-particle case

where a is the lattice parameter and the barrier between two neighboring potential minima is $2V_0$.

For a single particle on an active surface the tracer diffusion coefficient is known analytically [13]. Unfortunately, within this theory D_T can only be solved numerically. Only in the special cases of a very low friction or high friction an analytic approximation is available.

In the limit of high friction, $\eta \rightarrow \infty$, we have an accurate analytic approximation for D_T [4, 14]. Within this approximation the tracer diffusion coefficient for example along the x direction can be written as

$$D_T^{xx} = \frac{a^2 k_B T}{m\eta} \frac{\int_0^b \left\{ \int_0^a \exp[\beta V_A(\vec{r})] dx \right\}^{-1} dy}{\int_0^b \int_0^a \exp[-\beta V_A(\vec{r})] dx dy}, \quad (2.6.6)$$

where a and b are the lattice spacings in x and y directions, respectively, of a lattice formed by the minima of the surface potential. In an isotropic case both x and y directions are of course equivalent. Substituting the potential (2.6.5) yields

$$D_T = \frac{k_B T}{m\eta} I_0(V_0\beta)^{-2}, \quad (2.6.7)$$

where I_0 denotes the modified Bessel function of the first kind of order zero. For the potential (2.6.5) the requirement of high friction can be expressed as $\eta/\omega_0 \gg 1$, where $\omega_0 = (\pi/\sigma)\sqrt{V_0/m}$ is the frequency of the vibrational mode and σ is the diameter of the diffusing particle.

At the low friction limit when $\eta/\omega_0 \ll k_B T/V_0$ a simple approximate formula exists only for a one dimensional system [2]:

$$D_T = \frac{\pi k_B T}{2m\eta} \exp\left(-\frac{2V_0}{k_B T}\right). \quad (2.6.8)$$

However, the validity of this expression is limited to extremely low values of friction, which are not very common in surface physics.

2.7 Many-particle case

2.7.1 Lattice gas model

The most simple and widely used model of surface diffusion is the lattice gas (LG) model. The LG model is a discrete space model in which the

adparticles can be located only in discrete sites forming a lattice. In a sense this model describes a surface with a strongly binding surface potential which confines the adparticles to the lattice sites.

In the most simple version of the model, also called the Langmuir gas model, the only interaction between the particles is site exclusion, that is two particles can not occupy the same site at the same time. The particles attempt to make a jump to a randomly chosen nearest neighbor site at a certain attempt frequency. If the neighboring site is unoccupied the jump is always successful, if it is already occupied the jump is unsuccessful.

The LG approach has been immensely useful in diffusion studies due to its conceptual simplicity. It is relatively easy to model by computer simulations and it is even possible to obtain some analytical results. For finite coverages there exists a wealth of analytic and numerical diffusion studies for LG models of various systems [2–4, 15–21].

Within the Langmuir gas picture it is possible to solve the collective diffusion coefficient D_C exactly [15]. In general, we can decompose D_C as

$$D_C(\theta) = \frac{D_0(1 - \theta)}{\kappa_T(\theta)} f_C(\theta), \quad (2.7.1)$$

where $D_0 \equiv D(\theta = 0)$. The isothermal compressibility $\kappa_T(\theta)$ is a static factor and the second part $f_C(\theta)$ is a correlation factor containing all dynamical memory effects. In the lattice gas model it is customary to talk about coverage θ instead of the density. The coverage is defined as the proportion of the lattice sites that are occupied. The surprisingly simple result is that D_C is constant independent of coverage. This is due to the fact that $f_C(\theta) = 1$ and $\kappa_T(\theta) = (1 - \theta)$ exactly cancels out the coverage dependence.

The tracer diffusion coefficient D_T is more tricky to solve since the motion of the particles is not a simple random walk but rather it is highly correlated. A similar decomposition as for D_C above can also be written for D_T as

$$D_T(\theta) = D_0(1 - \theta) f_T(\theta), \quad (2.7.2)$$

where $f_T(\theta)$ is again a correlation factor as f_C above. A mean field result states that $f_T(\theta) = 1$ and the site blocking interaction causes a linear decay $D_T(\theta)/D_0 = (1 - \theta)$. Both diffusion coefficients are presented in Fig. 2.1. More accurate results for the tracer diffusion coefficient by Ferrando *et al.* [18] are also included.

2.7 Many-particle case

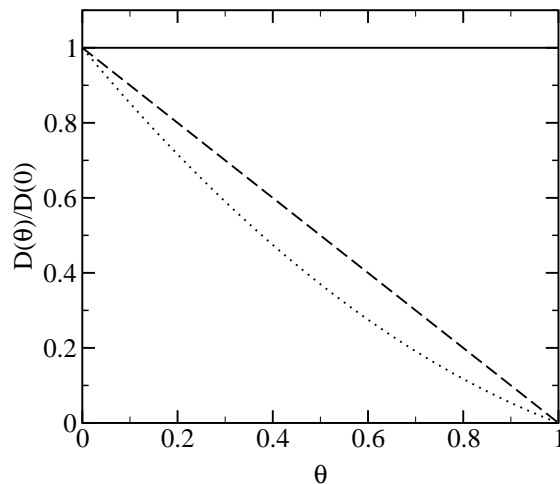


Figure 2.1: The diffusion coefficients in the Langmuir gas model. Solid line is the collective diffusion coefficient D_C , dashed line the mean field result $D_T = 1 - \theta$ for the tracer diffusion coefficient and the dotted line indicates data for D_T from Ref. [18]. The coverage θ is the proportion of lattice sites that are occupied.

2.7.2 Continuum case

In the continuum case the positions of the particles are not restricted to any discrete lattice sites, but they can move continuously on the surface. The motion of each particle in the system is governed by the Langevin equation

$$m \frac{d\vec{v}(t)}{dt} = -m\eta\vec{v}(t) + \vec{f}(t) + \vec{F}(t), \quad (2.7.3)$$

where $\vec{f}(t)$ is the total interaction force of the particle with other particles and the surface. In the absence of any interactions this equation is the same as Eq. (2.1.1) presented above.

A common choice for the particle-particle interaction potential is the Lennard-Jones potential or the purely repulsive $1/r^n$ potential. In this thesis we have studied the continuum model with the interaction potential of the form

$$V(r) = \epsilon \left(\frac{\sigma}{r} \right)^n, \quad (2.7.4)$$

where σ is the diameter of the particles and ϵ is a parameter. In the limit $n \rightarrow \infty$ this potential becomes the hard sphere potential. For n we have

chosen the commonly used value 12. In the simulations it is necessary to use a cutoff in this potential, otherwise the simulation becomes prohibitively slow because of the infinite range of this potential. A common choice for the cutoff is 2.5σ .

An interaction potential of the form (2.7.4) has the convenient property that in the smooth surface case without any external forces by making a simple scaling of the density the results obtained using one value of n can be translated to those of another value. The scaling works also for the limit $n \rightarrow \infty$ and thus results for a hard sphere system can be obtained by using a finite n in the simulations. The scaling is

$$\tilde{\rho} = \left(\frac{\epsilon}{k_B T} \right)^{2/n} \rho, \quad (2.7.5)$$

where $\rho = N/A$ is the density in a system of N particles, an area A , and interaction potential (2.7.4). The density $\tilde{\rho}$ is the corresponding density in the hard sphere system. If there is a surface potential in the system this scaling is not valid.

From the definition of the center of mass mobility D_{cm} (2.3.10) we can see that it measures the motion of the center of mass of all the particles. If there is no surface potential and the particle interactions preserve the momentum, the center of mass motion is of course completely unaffected by the particle-particle interactions and the center of mass mobility behaves as if the particles did not interact at all. In the case of a non-interacting system it is easy to show from the definition of D_{cm} that it does not depend on the density. If there is a surface potential in the system the particles can exchange momentum with the surface and this simple result does not hold any more.

Thus on a smooth surface the behavior of the collective diffusion coefficient is solely determined by the thermodynamic factor. As noted already above it is possible to extract the thermodynamic factor from an equation of state if one is available. For the hard sphere system on a smooth surface there are several approximations available in the literature. Perhaps the most compact formula is given by Boublik [22] for convex particles as

$$\frac{\rho}{S_0} = \frac{1 + 2\rho A_c(\gamma - 1)}{(1 - \rho A_c)^2} + \frac{2\rho A_c[1 + \rho A_c(\gamma - 1)]}{(1 - \rho A_c)^3}, \quad (2.7.6)$$

where the aspect ratio $\gamma = \pi R_c^2/A_c$, for convex particles of area A_c and

2.7 Many-particle case

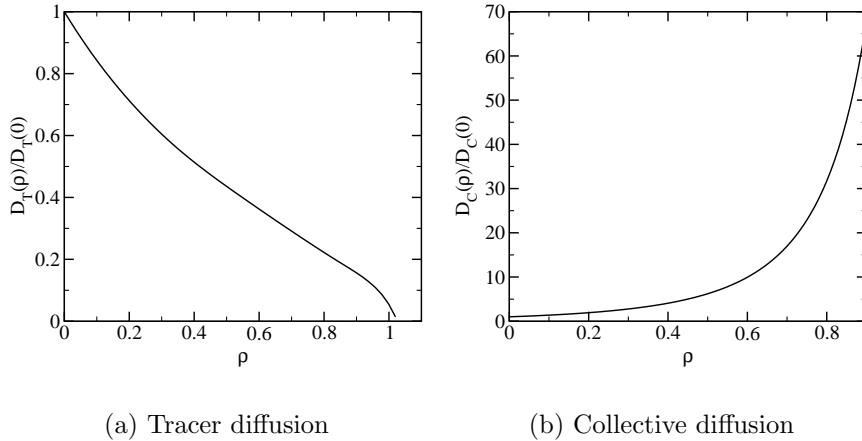


Figure 2.2: The tracer and collective diffusion coefficients in the smooth surface continuum model.

perimeter $2\pi R_c$. For the spheres $\gamma = 1$ and this reduces to

$$\frac{\rho}{S_0} = \frac{1}{(1 - \rho A_c)^2} + \frac{2\rho A_c}{(1 - \rho A_c)^3}. \quad (2.7.7)$$

In Publication II we have tested this expression and it agrees extremely well with the simulation results at densities below the freezing transition.

In analogy to the lattice gas model the tracer diffusion coefficient is harder to determine theoretically and no accurate analytic theory for it exists in the continuum case. In Fig. 2.2 we show the behavior of both diffusion coefficients schematically. This shows that there is a major difference between the lattice gas model and the continuum model. In the continuum model the center of mass mobility D_{cm} is a constant independent of density, whereas in the lattice gas model it is the collective diffusion coefficient D_C itself that does not depend on the coverage. The behavior of the tracer diffusion coefficient is qualitatively similar in both cases.

Chapter 3

Sedimentation of non-Brownian particles

3.1 Sedimentation dynamics

In this Section we consider a system of non-colloidal particles suspended in a fluid. The size of the particles is taken to be so large that the Brownian motion discussed in the previous Chapter is no longer important. An important aspect that we need to consider instead is the role of long ranged hydrodynamic interactions mediated by the fluid.

A measure of the relative importance of the Brownian diffusion in the system is given by the Péclet number. It is defined as the ratio of a typical velocity of the particles times the size of the particles to the diffusion coefficient of a single isolated particle

$$\text{Pe} = \frac{va}{D_T}, \quad (3.1.1)$$

where a is the radius of the colloidal particles, v their average velocity and D_T the tracer diffusion coefficient. In the non-Brownian sedimentation systems considered in this thesis the Péclet number is very large ($\text{Pe}^{-1} = 0$).

The motion of the fluid is governed by the Navier-Stokes equation

$$\rho_l \left[\frac{\partial \vec{u}}{\partial t} + (\vec{u} \cdot \nabla) \vec{u} \right] = -\nabla p + \eta \nabla^2 \vec{u} + \vec{f}, \quad (3.1.2)$$

Chapter 3. Sedimentation of non-Brownian particles

where ρ_l is the density of the fluid, \vec{u} is the velocity of the fluid, η the viscosity and p the pressure. The remaining force term \vec{f} includes all external forces like the effect of gravity. In addition to this we have the continuity equation

$$\nabla \cdot \vec{u} = 0, \quad (3.1.3)$$

which is here written for an incompressible fluid.

In some cases the inertial term $\rho_l(\vec{u} \cdot \nabla)\vec{u}$ on the left hand side of Eq. (3.1.2) can be ignored and thus the Navier-Stokes equation becomes the more simple Stokes equation

$$\rho_l \frac{\partial \vec{u}}{\partial t} = -\nabla p + \eta \nabla^2 \vec{u} + \vec{f}, \quad (3.1.4)$$

which is linear in \vec{u} and thus easier to handle. We can determine when this is the case by considering the ratio of the magnitude of the inertial term $|\rho_l(\vec{u} \cdot \nabla)\vec{u}| \propto \rho_l v^2/L$ to the viscous dissipative term $|\eta \nabla^2 \vec{u}| \propto \eta v/L^2$ on the right hand side of Eq. (3.1.2). This ratio defines the so-called Reynolds number

$$\frac{|\rho_l(\vec{u} \cdot \nabla)\vec{u}|}{|\eta \nabla^2 \vec{u}|} \propto \frac{vL\rho_l}{\eta} = \text{Re}, \quad (3.1.5)$$

where v is a typical velocity of the colloidal particles and L a characteristic length scale, which we assume to be related to the particle size. Thus at very small Reynolds numbers ($\text{Re} \ll 1$) the effect of inertia is negligible and the Stokes equation (3.1.4) is valid. In this thesis, however, we consider systems with finite Reynolds numbers and apply the full Navier-Stokes equation.

In solving the fluid equation of motion an important aspect concerns the boundary conditions on the surface of the colloidal particles. One condition in case of solid colloidal particles is that the fluid cannot pass through the surface of the particles, i.e. the velocity component normal to the particle surface must be equal to the velocity of the surface

$$\vec{u} \cdot \vec{n} = \vec{v}_s \cdot \vec{n}, \quad (3.1.6)$$

where \vec{v}_s is the velocity of the particle surface and \vec{n} a unit vector normal to the particle surface.

The other boundary condition is not quite so obvious. It has been shown experimentally that also the fluid velocity component parallel to the particle surface must equal the velocity of the surface

$$\vec{u} \times \vec{n} = \vec{v}_s \times \vec{n}. \quad (3.1.7)$$

3.1 Sedimentation dynamics

This is because the surface acts like a layer of fluid moving with velocity \vec{v}_s and the viscosity of the fluid prevents a discontinuity of the velocity between the fluid and the particle surface. This is called the no-slip boundary condition.

Let us first look at the motion of a single isolated spherical particle in the system. If the particle is initially at rest the gravity is going to accelerate it until the drag which is proportional to the particle velocity is equal to the gravitational force and the particle reaches a steady sedimentation velocity. The terminal velocity is called the Stokes velocity and in the limit $\text{Re} \ll 1$ it depends on the particle size and the fluid properties as

$$v_s(\rho) = \frac{2}{9} \frac{r^2(\rho_p - \rho_l)g}{\eta}, \quad (3.1.8)$$

where r is the radius of the particle, ρ_p the density of the particle, and g the gravitational acceleration.

When we have more than one particle in the system the situation becomes complicated because the particles will interact with one another through the hydrodynamic interactions mediated by the motion of the fluid. Again the system started at rest accelerates in the direction of the gravity until the drag of the fluid balances the gravitational force. After a certain time the system reaches a steady state in which the average sedimentation velocity does not increase anymore.

In the many-particle case the average sedimentation velocity in the steady state depends on the volume fraction of the sedimenting particles Φ . Increasing the volume fraction also increases the back flow of the fluid induced by the motion of the sedimenting particles. This makes the average sedimentation velocity decrease as a function of the volume fraction. The phenomenological Richardson-Zaki law [23] (RZ) describes the dependence of the sedimentation velocity on Φ as

$$\frac{v_s(\rho)}{v_s(0)} = (1 - \Phi)^{n_{RZ}}. \quad (3.1.9)$$

Values of the exponent n_{RZ} varying between 4.5 and 5.5 have been found to give good agreement with experiments in many systems. We show this with $n_{RZ} = 5.5$ in Fig. 3.1 along with our simulation results in a system with periodic boundary conditions in all directions. In this system it seems that the initial decrease in the sedimentation velocity is actually somewhat faster than the prediction given by the Richardson-Zaki law.

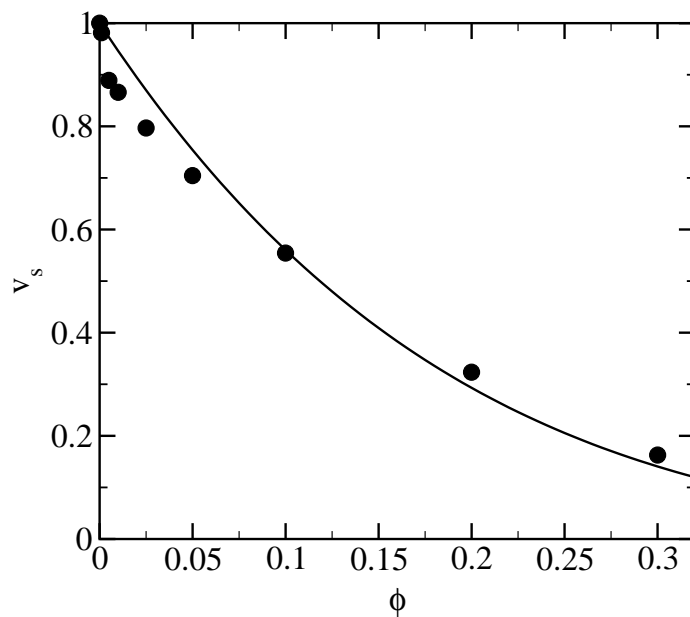


Figure 3.1: The sedimentation velocity in a system with periodic boundary conditions in all directions. The circles are our simulation results in a system with $Re = 0.5$ and the particle density was 2.5 times the fluid density. The solid line is the Richardson-Zaki law with $n_{RZ} = 5.5$.

3.1 Sedimentation dynamics

An interesting question concerns the fluctuations of the particle velocities in the steady state. Consider a system in the regime where the Stokes equation (3.1.4) is valid. A concentration fluctuation in this system gives rise to a velocity fluctuation decaying as $1/r$. The linearity of the Stokes equation implies that the velocity fluctuation in any given point in the fluid is given by a sum $\sum_i \vec{v}_i$ over all spatially distributed density fluctuations. If these individual contributions were independent the variance of the velocity σ_v^2 at the given point would clearly be a sum over squares of the individual contributions $\sum_i \vec{v}_i^2$. In a suspension where the volume fraction of the particles is $\Phi \propto N/L^3$ this sum has $N \propto L^3$ terms, where L is the linear size of the system. From the $1/r$ dependence it follows that each individual term goes like $\vec{v}_i^2 \propto L^{-2}$. This would imply that $\sigma_v^2 \propto L$, i.e. the velocity fluctuations diverge as the system size increases.

The divergence of the velocity fluctuations is surprising, and in fact, most experiments do not support it. Theoretical approaches range from arguing that the interpretation of the experiments is wrong to trying to find different kinds of screening mechanisms that would suppress the velocity fluctuations in larger systems. Thus this matter is still an open question and is currently under intense investigation and debate. [24]

Since the sedimentation system is not in equilibrium the definitions of the diffusion coefficients given above are not useful. Instead the system is in a steady state and we can define the tracer diffusion coefficient D_T through the velocity fluctuations. We define the velocity fluctuation autocorrelation function as

$$C_\alpha(t) \equiv \langle \delta v_\alpha(t) \delta v_\alpha(0) \rangle, \quad (3.1.10)$$

where $\delta v_\alpha(t) \equiv v_\alpha(t) - \langle v_\alpha \rangle$ and α refers to the Cartesian component of the velocity of a sedimenting particle \vec{v} . For the direction parallel to the gravity $\langle v_\alpha \rangle$ equals the average sedimentation velocity of the system and for directions perpendicular to the gravity it is of course zero. The brackets $\langle \rangle$ denote here an average over the steady state. The tracer diffusion coefficient is then defined in the Green-Kubo form analogous to Eq. (2.2.6) as

$$D_{T\alpha} \equiv \int_0^\infty C_\alpha(t) dt. \quad (3.1.11)$$

This definition is almost the same as the corresponding Eq. (2.2.6) given above for the equilibrium case, except we are now looking at the system in a frame of reference moving with the particles with the average sedimentation

velocity. Instead of equilibrium ensemble averages we are averaging over the steady state distribution.

3.2 The model

The non-linearity and complicated boundary conditions make the problem of sedimentation analytically unsolvable except in some very simple cases. For the same reasons also numerical treatment possesses tremendous practical problems. Standard methods for solving the Navier-Stokes equation exist but the main challenges in this particular problem are: (i) the proper treatment of the no-slip boundary conditions without compromising the efficiency of the fluid solver, and (ii) calculation of the forces and torque exerted by the fluid on the particles.

A multitude of models have been developed to simulate sedimentation systems. One class is the finite volume and finite element methods [25], which implement the no-slip boundary conditions on the particle surfaces. The problem in these methods is that since the particles are moving in the fluid the boundary conditions require constant updating, rendering these techniques computationally very costly.

A more microscopic description of the problem is provided by the Lattice-Boltzmann method [26]. This method has been shown to be very versatile in modeling the fluid-solid boundary [27]. Due to the length and time scales of the problem the even more microscopic treatment using a traditional Molecular Dynamics algorithm is not possible.

A large and important class of techniques concentrate on solving the Stokes equation (3.1.4). Thus these techniques [28, 29] are not useful in modeling systems with finite Reynolds numbers, which we are interested in.

The model we have used in addressing this problem is the one developed by Höfler and Schwartz [30]. This model uses the full Navier-Stokes equation and thus it can be applied to finite Reynolds number systems. Its salient feature is the numerically convenient and efficient approach to implement the no-slip boundary condition on the particle surface in combination with a conventional flow solver. In its present form the model can treat non-Brownian ($Pe^{-1} = 0$) systems with Reynolds numbers Re between 0.01 and 10, that is in the regime where the inertia of the fluid cannot be neglected

3.2 The model

but the flow is still laminar. With the chosen Reynolds number $\text{Re} = 0.5$ the accessible volume fractions Φ are within the dilute and moderate regimes.

The simulation process can be divided into three stages: (i) the motion of the fluid, (ii) the motion of the sedimenting particles, and (iii) their coupling. The numerical solution of the first two stages are standard and there exists several methods in the literature for them. The most challenging part is handling the coupling of the fluid and the particles correctly. Especially in case of moving bodies the explicit treatment of the no-slip boundary condition (3.1.7) is very costly.

As mentioned above, the motion of the fluid is governed by the Navier-Stokes equation (3.1.2). In addition, the fluid is taken to be incompressible, that is $\nabla \cdot \vec{u} = 0$. The incompressibility is not essential from the point of view of the coupling of the particles and the fluid, it only influences the solution of the fluid motion. The numerical solution of the Navier-Stokes equation is accomplished in a standard way discretizing the pressure and velocity fields, p and \vec{u} respectively, in an orthogonal lattice and using a finite-difference method to discretize the differentials. In addition the time is discretized in constant time steps and solution of the Navier-Stokes equation satisfying the continuity equation is found in the usual way.

In coupling the particle motion to the motion of the fluid we add in the Navier-Stokes equations a force term, which makes the fluid act inside the particles like a rigid body. The particle is effectively split into two parts: the portion of fluid inside the particle and a rigid particle template.

The constraint force that is applied in the Navier-Stokes equation is obtained in the following way. First we introduce a number n_i of reference points \vec{r}_{ij}^r , $j = 1, \dots, n_i$ distributed over the volume of the particle template i . The position \vec{r}_{ij}^r is defined relative to the center of mass of the particle template and the actual spatial coordinate \vec{x}_{ij}^r of the reference point is given by

$$\vec{x}_{ij}^r(t) = \vec{x}_i(t) + \mathbf{O}_i(t) \cdot \vec{r}_{ij}^r, \quad (3.2.1)$$

where $\vec{x}_i(t)$ is the position of the template and the matrix \mathbf{O}_i describes the orientation of the particle.

With each reference point in the template we associate a marker at \vec{x}_{ij}^m , $j = 1, \dots, n_i$ that moves with the fluid

$$\dot{\vec{x}}_{ij}^m = \vec{u}(\vec{x}_{ij}^m), \quad (3.2.2)$$

where \vec{u} is the fluid velocity, which is interpolated to an off-lattice site.

The constraint force field \vec{f} applied in the Navier-Stokes equation can now be written in terms of the displacement of the markers from their corresponding reference points in the template $\vec{\xi}_{ij} = \vec{x}_{ij}^m - \vec{x}_{ij}^r$. The effect of this force field \vec{f} is to make the markers and thus also the fluid to follow the motion of the rigid template. The force field has been chosen in the model in the form of a spring force as

$$\vec{f}_{ij}(\vec{x}) = (-k\vec{\xi}_{ij} - 2\gamma\dot{\vec{\xi}}_{ij})\delta(\vec{x} - \vec{x}_{ij}^m), \quad (3.2.3)$$

where k is a spring constant, γ a damping constant and δ the Dirac delta function. The force field \vec{f} is then obtained by summing over all particles i and all reference points j .

Finally, the motion of the template is determined from the Newton's equation of motion. The forces acting on the template are the gravitational force, particle-particle interactions and the spring forces between the template reference points and the fluid markers, that is

$$\vec{F}_{ij} = k\vec{\xi}_{ij} + 2\gamma\dot{\vec{\xi}}_{ij}. \quad (3.2.4)$$

It is worth pointing out that the buoyancy of the particle is correctly accounted for because the particle mass equals the template mass plus the mass of the fluid inside the particle and the gravity affects only the mass of the template.

In most non-Brownian suspensions the direct interactions between the sedimenting particles are negligible because at short range the hydrodynamic lubrication forces are far stronger. Because of the finite discretization lattice such lubrication forces are not correctly accounted for and therefore we add an explicit short range interaction between the particles to prevent particle overlaps. Define the overlap between particles i and k as $\vec{\zeta}_{ik} = (2r - |\vec{x}_i - \vec{x}_k|)\vec{e}_{ik}$, with \vec{e}_{ik} denoting the unit vector pointing from k to i . Then the particle-particle interaction force is taken to be

$$\vec{F}_{ik}^p = -k_p\vec{\zeta}_{ik}. \quad (3.2.5)$$

This type of interaction mimics the lubrication forces sufficiently accurately.

Chapter 4

Methods

4.1 Molecular Dynamics

For the treatment of colloidal systems without hydrodynamic interactions we use the Molecular Dynamics method. In this method one solves numerically the classical equations of motion of the system and obtains its time evolution. In a sense Molecular Dynamics is like performing a simulated experiment in which the particle positions and momenta at any given time can be observed exactly. There are many numerical schemes through which this can be accomplished but clearly no numerical algorithm can provide an exact solution of the trajectories for long times. Fortunately one is usually interested in the statistical properties of the system and not in the exact classical trajectories of the particles. One needs to make sure that the energy of the system stays at the desired level and the microcanonical ensemble is thus sampled accurately enough.

The motion of the system is governed by the Newton's equations of motion

$$\ddot{\vec{r}}_i = \vec{f}_i/m_i \quad (4.1.1)$$

and

$$\vec{f}_i = -\nabla_{\vec{r}_i} V, \quad (4.1.2)$$

where V is the potential energy of the system and it includes the particle-particle interaction potential as well as any external potentials.

The numerical algorithm for solving these equations of motion in this thesis is based on the Velocity Verlet algorithm [31]. This algorithm gives the

positions and velocities of the particles in discrete time steps as

$$\vec{r}(t + \delta t) = \vec{r}(t) + \delta t \vec{v}(t) + \frac{1}{2} \delta t^2 \vec{a}(t) \quad (4.1.3)$$

and

$$\vec{v}(t + \delta t) = \vec{v}(t) + \frac{1}{2} \delta t [\vec{a}(t) + \vec{a}(t + \delta t)], \quad (4.1.4)$$

where \vec{r} , \vec{v} and \vec{a} are the position, the velocity, and the acceleration of all the particles, respectively. In this algorithm the positions and the velocities of the particles are readily available and it is therefore well suited for studying the dynamics and diffusion properties of the system.

In our case, instead of solving the Newton's equations of motion (4.1.1) we are really interested in the Langevin dynamics (2.7.3) generating a canonical ensemble. The Velocity Verlet algorithm can be modified to include the random fluctuations and the friction term of the Langevin equation in the following way [31]. The updating algorithms for the position and the velocity become

$$\vec{r}(t + \delta t) = \vec{r}(t) + c_1 \delta t \vec{v}(t) + c_2 \delta t^2 \vec{a}(t) + \delta \vec{r}^G \quad (4.1.5)$$

and

$$\vec{v}(t + \delta t) = c_0 \vec{v}(t) + (c_1 - c_2) \delta t \vec{a}(t) + c_2 \delta t \vec{a}(t + \delta t) + \delta \vec{v}^G, \quad (4.1.6)$$

where $\delta \vec{r}^G$ and $\delta \vec{v}^G$ are random variables from a bivariate Gaussian distribution with zero means and variances given by

$$\sigma_r^2 = \delta t^2 \frac{k_B T}{m} (\eta \delta t)^{-1} [2 - (\eta \delta t)^{-1} (3 - 4e^{-\eta \delta t} + e^{-2\eta \delta t})] \quad (4.1.7)$$

and

$$\sigma_v^2 = \frac{k_B T}{m} (1 - e^{-2\eta \delta t}), \quad (4.1.8)$$

and a correlation coefficient c_{rv}

$$c_{rv} \sigma_r \sigma_v = \delta t \frac{k_B T}{m} (\eta \delta t)^{-1} (1 - e^{-\eta \delta t})^2. \quad (4.1.9)$$

Here T is the temperature, k_B Boltzmann constant, m the particle mass, η the friction coefficient, and δt the simulation time step. The coefficients c_i appearing in Equations (4.1.5) and (4.1.6) are given by

$$c_0 = e^{-\eta \delta t}, \quad (4.1.10)$$

4.2 Monte Carlo methods

$$c_1 = (\eta \delta t)^{-1}(1 - c_0), \quad (4.1.11)$$

and

$$c_2 = (\eta \delta t)^{-1}(1 - c_1). \quad (4.1.12)$$

After determining the random components $\delta\vec{r}^G$ and $\delta\vec{v}^G$ the algorithm is implemented in the usual way. In the simulations we have generated the random numbers needed with the RANMAR random number generator [32, 33].

4.2 Monte Carlo methods

With the ever increasing computing power of the modern computers the Monte Carlo simulation method has become very popular in the field of statistical physics as well as in many other disciplines. In general, the name Monte Carlo has been attached to any method that somehow uses random numbers. In physics Monte Carlo methods can be classified as either static or dynamic methods [34].

In statistical physics Monte Carlo is a method of evaluating thermal average values of quantities in a given system. A thermal average of a given quantity $A(\mathbf{x})$ is defined in the canonical ensemble as

$$\langle A(\mathbf{x}) \rangle = \frac{1}{Z} \int \exp[-\mathcal{H}(\mathbf{x})/k_B T] A(\mathbf{x}) d\mathbf{x}, \quad (4.2.1)$$

where $Z = \int \exp[-\mathcal{H}(\mathbf{x})/k_B T] d\mathbf{x}$. Here $\mathbf{x} \in \Omega$ is a vector of the phase space Ω . The dimension of the phase space equals twice the number of degrees of freedom in the system. As can be seen from Eq. (4.2.1) the normalized Boltzmann factor $\frac{1}{Z} \exp[-\mathcal{H}(\mathbf{x})/k_B T]$ plays the role of a probability distribution describing the probability with which a configuration \mathbf{x} occurs in a thermal equilibrium.

In general, carrying out the integration in Eq. (4.2.1) is not possible, however. Even a numerical evaluation of the integral would be a prohibitively large task if the system has a large number of degrees of freedom. A static Monte Carlo algorithm reduces the numerical work by generating a random set of uncorrelated phase space points $\{\mathbf{x}_1, \mathbf{x}_2, \dots, \mathbf{x}_N\}$ and evaluating the integral based on these representative points only

$$\langle A(\mathbf{x}) \rangle \approx \frac{\sum_{i=1}^N \exp[-\mathcal{H}(\mathbf{x}_i)/k_B T] A(\mathbf{x}_i)}{\sum_{i=1}^N \exp[-\mathcal{H}(\mathbf{x}_i)/k_B T]}. \quad (4.2.2)$$

A dynamical Monte Carlo algorithm, like the ones used in this work, is based on a stochastic process, which generates a Markov chain of points in the phase space. A Markov chain is a chain of states in which the next state in the chain depends only on the present state and not on the previous ones. For simplicity we can assume that the phase space is discrete. Provided that the transition probabilities p_{xy} between two states $\mathbf{x} \in \Omega$ and $\mathbf{y} \in \Omega$ have been selected properly the equilibrium distribution π of the stationary Markov process is the desired Boltzmann distribution and the generated states can be used to evaluate the thermal average of $A(\mathbf{x})$ simply as

$$\langle A(\mathbf{x}) \rangle \approx \frac{1}{N} \sum_{i=1}^N A(\mathbf{x}_i), \quad (4.2.3)$$

that is by taking an average of the values of A in the generated configurations \mathbf{x}_i .

There are two essential properties that the Markov process used must have. First, the process has to be ergodic, i.e.

$$\forall \mathbf{x}, \mathbf{y} \in \Omega \exists n > 0 \text{ such that } p_{xy}^{(n)} > 0. \quad (4.2.4)$$

Here $p_{xy}^{(n)}$ is the n -step transition probability from \mathbf{x} to \mathbf{y} . This simply means that any configuration \mathbf{y} can be reached starting from any other configuration \mathbf{x} by a finite number of steps. Secondly, the process has to be stationary, i.e.

$$\forall \mathbf{y} \in \Omega \sum_{\mathbf{x} \in \Omega} \pi_{\mathbf{x}} p_{xy} = \pi_{\mathbf{y}}, \quad (4.2.5)$$

the transition probabilities being normalized to $\sum_{\mathbf{y} \in \Omega} p_{xy} = 1$ as usual. If these conditions are fulfilled it can be shown that π is a unique stationary distribution of the Markov process [34]. If, in addition, the process is aperiodic, that is

$$\forall \mathbf{x}, \mathbf{y} \in \Omega \ p_{xy}^{(n)} > 0 \ \forall n \text{ sufficiently large}, \quad (4.2.6)$$

then the probability distribution converges to π irrespective of the initial state, that is $\lim_{n \rightarrow \infty} p_{xy}^{(n)} = \pi_{\mathbf{y}}$ for all \mathbf{x} . This gives valuable freedom in the construction of the simulation since the simulation can be started at an arbitrary point in the phase space.

A practical way of implementing the stationarity condition and satisfying condition (4.2.5) in a computer algorithm is to use the following stronger

4.2 Monte Carlo methods

condition called the detailed balance condition:

$$\pi_x p_{xy} = \pi_y p_{yx}. \quad (4.2.7)$$

One can easily verify that this is a sufficient condition to satisfy the stationarity condition by substituting Eq. (4.2.7) into Eq. (4.2.5) and taking into account the normalization of the probabilities.

Towards the end of making this algorithm a little more explicit and stating the condition for obtaining the Boltzmann distribution as the equilibrium distribution π let us decompose the transition probability into two parts. We write $p_{xy} = \alpha_{xy} \times a_{xy}$, where α_{xy} is the probability to make a trial move from \mathbf{x} to \mathbf{y} and a_{xy} is the probability that the trial move is accepted.

In the original form of the algorithm by Metropolis *et al.* [35] the trial probabilities were chosen to be symmetric, i.e. $\alpha_{xy} = \alpha_{yx}$. In the canonical ensemble we know that the probability of state \mathbf{x} of the system is proportional to the Boltzmann factor $\pi_x \propto \exp[-\beta\mathcal{H}(\mathbf{x})]$. Then it follows from the detailed balance condition (4.2.7) that

$$\frac{a_{xy}}{a_{yx}} = \frac{\pi_y}{\pi_x} = \exp[-\beta(\mathcal{H}(\mathbf{y}) - \mathcal{H}(\mathbf{x}))]. \quad (4.2.8)$$

There are, of course, many possible ways of choosing the acceptance probabilities so that they satisfy this condition. The original choice made by Metropolis *et al.* [35] was to always accept a move to a lower energy state and only some of the moves to a higher energy state resulting in the following acceptance probabilities in the canonical ensemble

$$a_{xy} = \begin{cases} \exp[-\beta \delta E] & , \text{ if } \pi_y < \pi_x; \\ 1 & , \text{ if } \pi_y \geq \pi_x, \end{cases} \quad (4.2.9)$$

where $\delta E = \mathcal{H}(\mathbf{y}) - \mathcal{H}(\mathbf{x})$. Another widely used choice is the symmetric Kawasaki criterion

$$a_{xy} = \frac{1}{2} [1 - \tanh(\frac{1}{2}\beta \delta E)]. \quad (4.2.10)$$

In practice, one draws a random number from a uniform $[0, 1]$ -distribution and accepts the trial move if the random number is smaller than a_{xy} .

In constructing the actual algorithm one has to design the trial moves such that the system as efficiently as possible explores the phase space. If the attempted moves are too small most of the attempts probably get accepted

but it takes a lot of time for the system to move from one point of the phase space to another and thus very long simulation runs are necessary. If, on the other hand, the attempted moves are too large they hardly ever get accepted. This computational efficiency of the algorithm can be measured by investigating the autocorrelation time of an observable A and calculating how much CPU time does it take to create from one configuration a statistically independent new configuration.

It is also important to keep in mind that since the algorithm allows considerable freedom in the construction of the trial moves the evolution of the system does not describe any real physical dynamics. In fact, in order to optimize the algorithm it is often necessary to use highly unphysical trial moves. In conclusion the Monte Carlo algorithm is highly effective in evaluating static quantities, but it may not be suitable for simulating the dynamics of the system.

4.3 Computation of the diffusion coefficients

4.3.1 The memory expansion method

Using the definitions (2.2.1) and (2.3.10) directly to evaluate the diffusion coefficients can be a tedious task due to the lack of self averaging [36]. In this Section we present the memory expansion method [37], which is a more efficient way. This method is suitable for the evaluation of any transport coefficients, such as the collective diffusion coefficient D_C or the tracer diffusion coefficient D_T . It has been shown that this method can speed up the computation of the collective diffusion coefficient D_C by up to two orders of magnitude. For the tracer diffusion coefficient the speed-up is not quite as significant. This method is suited for both Monte Carlo and Molecular Dynamics simulations, although in the work reported in this thesis all the dynamic quantities have been obtained using the Molecular Dynamics method.

The basis for the derivation of the memory expansion is the Green-Kubo formalism [6]. Within this formalism a transport coefficient, such as a diffusion coefficient, can be expressed in terms of time correlations of the spatial μ, ν components of a “current flux” $\vec{J}(t)$:

$$T_{\mu\nu} = A \int_0^\infty \langle J_\mu(t) J_\nu(0) \rangle. \quad (4.3.1)$$

4.3 Computation of the diffusion coefficients

In isotropic systems all directions are equivalent and the time correlation function above can be written as $\langle \vec{J}(t) \cdot \vec{J}(0) \rangle$. For the tracer diffusion coefficient the flux $\vec{J}(t)$ is the velocity of the tracer particle and (4.3.1) becomes Eq.(2.2.6). For the collective diffusion coefficient A is proportional to the thermodynamic factor and $\vec{J}(t)$ is the velocity of the center of mass of all the particles. Thus in this case Eq. (4.3.1) is equivalent to Eq. (2.3.5).

Let us first look at the memory expansion for the collective diffusion coefficient D_C . As already mentioned above the flux $\vec{J}(t)$ is the total flux of all the particles $\vec{J}(t) = \sum_{i=1}^N \vec{v}_i(t)$, where $\vec{v}_i(t)$ is the velocity of a particle i at time t . The current flux correlation function in (4.3.1) can also be presented in terms of the center of mass coordinates of the particles, defined as $\vec{R}(t) = \sum_{i=1}^N [\vec{r}_i(t) - \vec{r}_i(0)]$, where $\vec{r}_i(t)$ is the position of the particle i at time t . In this form the collective diffusion coefficient was given by Eq. (2.3.10) presented in Section 2.3, which we reproduce here for convenience

$$D_C = \frac{\rho}{S_0} D_{cm} = \frac{\rho}{S_0} \lim_{t \rightarrow \infty} \frac{1}{2Ntd} \langle |\vec{R}(t)|^2 \rangle. \quad (4.3.2)$$

Next we divide the time t into M time intervals of length τ_0 and discretize the center of mass coordinate correspondingly at times $t_m = m\tau_0$ with $m = 0, 1, \dots, M$. Choosing the coordinates such that $\vec{R}(0) = 0$ we have $\vec{R}(t) \equiv \vec{R}(M\tau_0) = \sum_{m=0}^{M-1} \delta\vec{R}(t_m)$, where $\delta\vec{R}(t_m) = \vec{R}(t_{m+1}) - \vec{R}(t_m)$ is the change in the position of the center of mass between two consecutive observations at times t_m and t_{m+1} . Using this notation D_{cm} in Eq. (4.3.2) can be written as

$$D_{cm} = \lim_{M \rightarrow \infty} \frac{1}{2dNM\tau_0} \left[M \langle \delta\vec{R}(t_m) \cdot \delta\vec{R}(t_m) \rangle + 2 \sum_{k=1}^{M-1} (M-k) \langle \delta\vec{R}(t_m) \cdot \delta\vec{R}(t_{m+k}) \rangle \right], \quad (4.3.3)$$

where the averages $\langle \rangle$ are taken with respect to t_m . In here the time-dependent correlation functions depend only on the time differences. By denoting

$$C_C(t) \equiv \langle \delta\vec{R}(0) \cdot \delta\vec{R}(t) \rangle, \quad (4.3.4)$$

we can write this in the convenient form

$$D_{cm} = \frac{1}{2dN\tau_0} \left[C_C(0) + 2 \sum_{k=1}^{\infty} C_C(k\tau_0) \right]. \quad (4.3.5)$$

The first term $C_C(0) = \langle |\vec{R}(\tau_0) - \vec{R}(0)|^2 \rangle$ gives the average mean square displacement of \vec{R} for a time interval of length τ_0 . The following terms in the expansion measure the memory of additional displacements with respect to the initial one. If the center of mass follows a Markovian random statistics then $C_C(0)$ is the only non-zero term in the expansion, assuming τ_0 is larger than any microscopic time scale in the system. In interacting systems this is not true, however, and the terms $C_C(k\tau_0)$ for $k > 0$ are finite.

This formula is particularly efficient for evaluating the center of mass displacement from simulations such as those presented in this thesis. It also offers another advantage over that of utilizing Eq. (4.3.2) directly. It is easier to see when this expansion has converged when evaluating it numerically than it is when one tries to determine the long time limit of the slope of the mean square displacement as suggested by Eq. (4.3.2).

The parameter τ_0 in Eq. (4.3.5) is arbitrary and it is chosen to optimize the computational process. If it is chosen too small, redundant information is collected. On the other hand an overly large value leads to sampling values for C_C which are beyond its correlation time and thus are only noise.

For the tracer diffusion coefficient the derivation is very similar. A definition analogous to Eq. (4.3.2) for the tracer diffusion was given in Section 2.2 by Eq. (2.2.1), which we again reproduce here

$$D_T = \lim_{t \rightarrow \infty} \frac{1}{2dt} \langle |\vec{r}_i(t) - \vec{r}_i(0)|^2 \rangle. \quad (4.3.6)$$

By proceeding in the same way as with the center of mass mobility above an equation similar to Eq. (4.3.5) is obtained. Only now the correlation terms become

$$C_T(t) \equiv \langle \delta\vec{r}_i(0) \cdot \delta\vec{r}_i(t) \rangle, \quad (4.3.7)$$

where $\delta\vec{r}_i(t)$ is the change in the position of the particle i between two consecutive observations. The memory expansion for the tracer diffusion coefficient reads

$$D_T = \frac{1}{4\tau_0} \left[C_T(0) + 2 \sum_{k=1}^{\infty} C_T(k\tau_0) \right]. \quad (4.3.8)$$

This is similar to Eq. (4.3.5) and the discussion about the meaning of the terms given above in the case of D_{cm} also applies here. The advantage in efficiency is not quite as striking here as it is with the center of mass mobility but the ease of determining the convergence also applies in the case of tracer diffusion.

4.3 Computation of the diffusion coefficients

4.3.2 The Boltzmann-Matano method

The Boltzmann-Matano method [3,38] is a popular method to determine the collective diffusion coefficient. This method is based on observing how a system with uneven spatial density moves towards equilibrium. The simplest such process is the spreading of an initially step-like density distribution. Save the initial spreading, the system is close enough to equilibrium for the linear response to be approximately valid. When the resulting profile evolution is compared with the solution of the diffusion equation it is possible to extract $D_C(\rho)$ for all densities ρ from a single measurement. This method is applicable to both experimentally observed and simulated processes.

We start with a step-like density profile

$$\rho(x, y, t = 0) = \begin{cases} \rho_{max}, & \text{for } x < 0; \\ 0, & \text{for } x \geq 0; \end{cases} \quad (4.3.9)$$

and observe it evolving through time. Due to the symmetry of the system in the y -direction the process can be described by the one-dimensional diffusion equation

$$\frac{\partial \rho}{\partial t} = \frac{\partial}{\partial x} \left[D_C(\rho) \frac{\partial \rho}{\partial x} \right]. \quad (4.3.10)$$

Next we define a new variable η

$$\eta = x t^{-1/2}. \quad (4.3.11)$$

Substituting this into Eq. (4.3.10) yields

$$\frac{\partial \rho}{\partial t} = \frac{d\rho}{d\eta} \frac{\partial \eta}{\partial t} = -\frac{x}{2\sqrt{t^3}} \frac{d\rho}{d\eta} \quad (4.3.12)$$

and

$$\frac{\partial \rho}{\partial x} = \frac{1}{\sqrt{t}} \frac{d\rho}{d\eta}, \quad (4.3.13)$$

and furthermore

$$\frac{\partial}{\partial x} \left(D_C \frac{\partial \rho}{\partial x} \right) = \frac{1}{\sqrt{t}} \frac{d}{d\eta} \left(D_C \frac{1}{\sqrt{t}} \frac{d\rho}{d\eta} \right) = \frac{1}{t} \frac{d}{d\eta} \left(D_C \frac{d\rho}{d\eta} \right). \quad (4.3.14)$$

Putting all these together we see that (4.3.10) becomes an ordinary differential equation and that ρ can be expressed in terms of just one variable η

$$-\frac{\eta}{2} \frac{d\rho}{d\eta} = \frac{d}{d\eta} \left(D_C(\rho) \frac{d\rho}{d\eta} \right). \quad (4.3.15)$$

Integrating this with respect to η and taking into account the boundary condition that initially ρ is a constant yields a useful expression for D_C

$$D_C(\rho) = -\frac{1}{2} \left(\frac{d\eta}{d\rho} \right)_\rho \int_0^\rho \eta d\rho'. \quad (4.3.16)$$

Plugging into this the density $\rho(\eta)$ obtained from either a simulation or an experiment we can evaluate $D_C(\rho)$ for all densities below ρ_{max} .

To obtain the true equilibrium diffusion coefficient with this method one must be careful, however. It has been shown [39] that in the presence of ordered phases or close to phase boundaries the obtained diffusion coefficient $D_C(\rho)$ is going to depend strongly on time regime chosen for analysis. This is due to the interplay between spreading and phase-ordering kinetics and is reflected in enhanced particle number fluctuations with respect to the equilibrium case. The systems studied in this thesis are not close to boundaries of any ordered phases.

4.4 Computation of the thermodynamic factor

The thermodynamic factor S_0 , which was defined above by (2.3.8) is an important ingredient in computing the collective diffusion coefficient. Since the thermodynamic factor is sensitive to the system size and we really want to measure it in the thermodynamic limit a trick is needed. We use an extrapolation method [40] to make sure the results are not affected by our finite system size. We compute the thermodynamic factor in several subsystems of the total system and then extrapolate to an infinite size.

The thermodynamic factor is evaluated by computing the structure factor $S(k) = S(k, 0)$. The smallest k value that can be reached is of course dictated by the system size and therefore we have to evaluate $S(k)$ at the smallest possible k values and then extrapolate to $k = 0$. This is done in all of the subsystems separately and from the results obtained in this way another extrapolation is made to an infinite system size.

The computation of $S(k)$ is performed by sampling the Fourier transform of the density as

$$S(k) = \frac{1}{N} \left\{ \left\langle \left[\sum_{i=1}^N \cos(kx_i) \right]^2 \right\rangle + \left\langle \left[\sum_{i=1}^N \sin(kx_i) \right]^2 \right\rangle \right\}, \quad (4.4.1)$$

4.4 Computation of the thermodynamic factor

where N is the number of particles and x_i is the x coordinate of the i th particle. In an isotropic system x and y directions are equivalent and the y direction provides us with another measurement of $S(k)$, which is independent of the results obtained in the x direction.

Chapter 5

Results

5.1 Continuum limit

In Publication II we have studied the behavior of the diffusion coefficients in a two dimensional system of hard disks on a smooth surface. This system is theoretically interesting due to its conceptual simplicity and some of its properties have been solved analytically.

The phase diagram of the system is very simple. At low densities the system is in a liquid phase, while beyond a certain transition density it freezes. For a true hard sphere system this freezing takes place at a density of $\rho = 0.887$ [40, 41]. As was explained in Section 2.7.2 in simulations we can use a softer potential of the form (2.7.4) and use the scaling (2.7.5) to obtain the hard sphere results. However, the transition density does not scale according to (2.7.5) and the freezing of the $n = 12$ potential system takes place at a slightly higher scaled density at $\tilde{\rho} = 0.986$ [41].

The nature of the freezing transition is not known for certain but simulation results suggest that it would be of the Kosterlitz-Thouless-Halperin-Nelson-Young type [42] with both the hard sphere potential [43] and the $n = 12$ potential [44, 45]. However, in this thesis we do not concern ourselves with the freezing transition but study the dynamics of the system in the liquid phase only.

By computing the tracer diffusion coefficient D_T at one density using both $n = 6$ and $n = 12$ we checked that the results for D_T can be scaled according to Eq. (2.7.5). Subsequently we have run the simulations using the $n = 12$

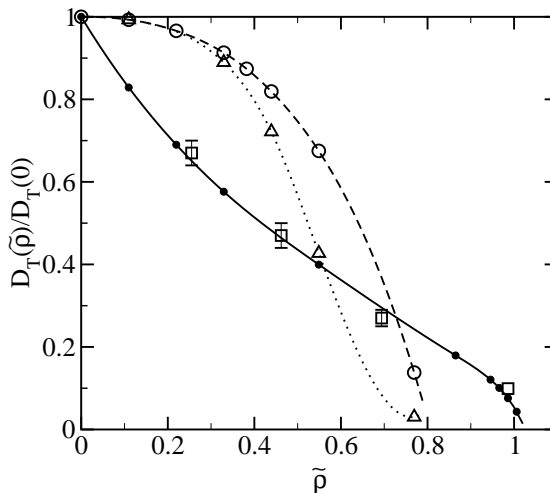


Figure 5.1: The normalized tracer diffusion coefficient of hard spheres on a smooth surface. Solid circles are our simulation data, squares reference data from Löwen [41, 46], open circles and triangles represent the mode-mode coupling approximation results. All lines are spline fits and are intended as guides to the eye only. Here and in all following Figures the error bars are smaller than the size of the symbols when not explicitly shown.

potential and present the results here in units which have been scaled to correspond to the hard sphere system.

In Table 5.1 and in Fig. 5.1 we present our results for the tracer diffusion coefficient on a smooth surface. The results have been normalized by the tracer diffusion coefficient at the zero density limit as given by Eq. (2.2.2). It is seen that D_T is a monotonically decreasing function of the density as expected from simple blocking and back-scattering arguments. As stated above in Section 2.7.2 no quantitative theoretical explanation for the density dependence of D_T exists. In Fig. 5.1 we also present the results of a mode-mode coupling approximation [47, 48] but as can be seen, they are not in good quantitative agreement with the simulation results.

Löwen has proposed a dynamical criterion for freezing based on the value of $D_T(\rho)/D_T(0)$ at the freezing density [41]. He has studied the behavior of D_T with different interaction potentials and finds that in 2D at freezing $D_T(\rho)/D_T(0)$ attains a universal value of 0.086. Our value of 0.0759 in the system with $1/r^{12}$ type of interaction is actually in better agreement with this criterion than the value obtained by Löwen in a smaller system.

5.2 The influence of an external potential

| Present results | | | | Löwen <i>et al.</i> | |
|-----------------|----------------------------|----------------|----------------------------|---------------------|----------------------------|
| $\tilde{\rho}$ | $D_T(\tilde{\rho})/D_T(0)$ | $\tilde{\rho}$ | $D_T(\tilde{\rho})/D_T(0)$ | $\tilde{\rho}$ | $D_T(\tilde{\rho})/D_T(0)$ |
| 0 | 1 | 0.865 | 0.1794(5) | 0.255 | 0.67(3) |
| 0.110 | 0.829(1) | 0.946 | 0.121(3) | 0.462 | 0.47(3) |
| 0.220 | 0.6900(8) | 0.966 | 0.101(2) | 0.694 | 0.27(2) |
| 0.329 | 0.5762(5) | 0.986 | 0.0759(4) | 0.986 | 0.099(3) |
| 0.549 | 0.3996(9) | 1.006 | 0.0431(8) | | |

Table 5.1: Numerical values of the normalized tracer diffusion coefficient for 2D hard disks from simulations and from Refs. [41, 46] by Löwen *et al.*

In the case of the collective diffusion coefficient it was already pointed out in Section 2.7.2 that the center of mass mobility D_{cm} does not depend on the density on a smooth surface. Thus according to Eq. (2.3.10) the density dependence of the collective diffusion coefficient D_C is completely determined by the thermodynamic factor ρ/S_0 . We plot our simulation data in Fig. 5.2 and compare it with the Boublik approximation Eq. (2.7.7). Also presented in the Figure is a virial expansion result by Van Rensburg [49]. The data are also given in Table 5.2. We can see that all the approximations agree perfectly with our simulation results up to densities of about $\tilde{\rho} = 0.7$ and even beyond that the discrepancy is of the order of the error estimate in the simulations.

5.2 The influence of an external potential

An interesting question is the relation of the continuum model to the widely used lattice gas model presented in Section 2.7.1. In the lattice gas model the particles' positions are restricted to lattice sites and therefore this model can be considered to be an approximation of a system in which a surface potential confines the particles into potential minima that form a lattice. The stronger the confining potential the more closely one would expect the behavior of the continuum model to be to that of the lattice gas model.

The validity of the lattice gas approximation for many-particle diffusion has not been studied before. To this end in Publication IV we consider a continuum system with the surface potential of the form

$$V_A(x, y) = V_0 \left[\cos\left(\frac{2\pi x}{a}\right) + \cos\left(\frac{2\pi y}{a}\right) \right], \quad (5.2.1)$$

| $\tilde{\rho}$ | $D_C(\tilde{\rho})/D_C(0)$ | | | |
|----------------|----------------------------|---------|----------------|----------------|
| | Simulated | Boublik | Van Rensburg 1 | Van Rensburg 2 |
| 0 | 1 | 1 | 1 | 1 |
| 0.055 | 1.20(2) | 1.191 | 1.192 | 1.192 |
| 0.110 | 1.43(2) | 1.425 | 1.428 | 1.428 |
| 0.165 | 1.74(3) | 1.713 | 1.722 | 1.722 |
| 0.220 | 2.08(2) | 2.072 | 2.091 | 2.091 |
| 0.275 | 2.56(3) | 2.523 | 2.556 | 2.557 |
| 0.329 | 3.17(3) | 3.085 | 3.137 | 3.140 |
| 0.384 | 3.94(5) | 3.821 | 3.897 | 3.905 |
| 0.440 | 4.93(5) | 4.801 | 4.902 | 4.926 |
| 0.550 | 8.1(3) | 7.813 | 7.877 | 8.034 |
| 0.865 | 42(7) | 50.95 | 34.11 | 41.19 |

Table 5.2: Numerical values of the normalized collective diffusion coefficient for 2D hard disks from simulations. In addition to our simulation data we also present values calculated with the Boublik formula (2.7.7) and data calculated from the virial expansion of Ref. [49]. The data in the column labeled Van Rensburg 1 have been obtained using the first eight virial coefficients and the data in the column labeled Van Rensburg 2 using a Padé approximation for the ninth and tenth virial coefficient.

5.2 The influence of an external potential

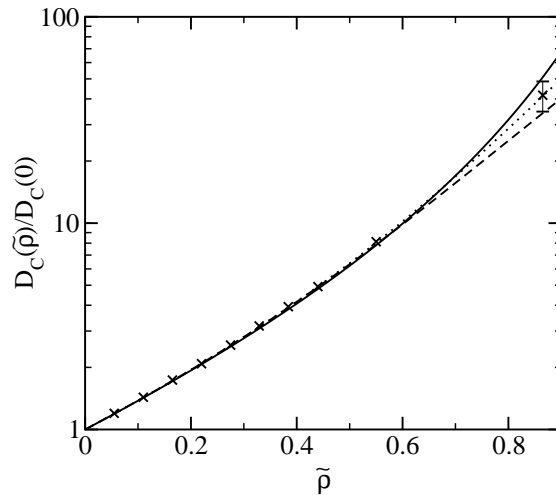
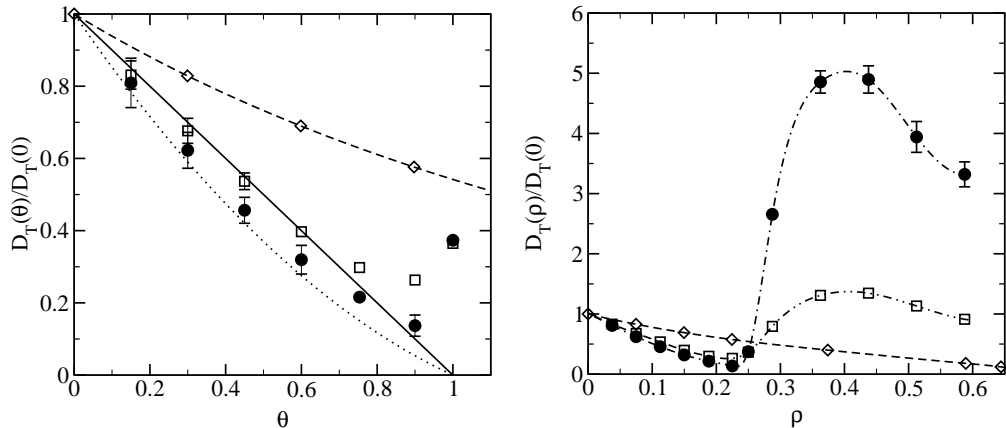


Figure 5.2: The collective diffusion coefficient for a hard sphere system on a smooth surface. The solid line is from Eq. (2.7.7), the dashed line is a virial expansions by Van Rensburg with first eight virial coefficients, and the dotted line with the ninth and tenth virial coefficient obtained using the Padé approximation.

where a is the lattice parameter and the barrier between two neighboring potential minima is $2V_0$. First we study the system in the high friction regime $\eta/\omega_0 \gg 1$, where $\omega_0 = (\pi/\sigma)\sqrt{V_0/m}$ is the frequency of the vibrational mode. In this regime the particles only jump to the neighboring minima and there are virtually no longer jumps or recrossing events. Under such conditions the Langmuir lattice gas model is expected to approximate well the continuum model. The lattice parameter a we have chosen to equal twice the diameter of the particles σ . With this choice two particles cannot occupy the same well and particles in neighboring wells interact relatively little. The temperature is set at $k_B T = 0.1$ in all cases.

In Figure 5.3 we present behavior of the tracer diffusion coefficient D_T . Again the same data are presented in Table 5.3. The coverage θ is defined as the proportion of lattice sites occupied in the lattice gas model and as the proportion of the number of particles to the number of potential minima in the continuum model. The lattice gas model is of course only defined up to $\theta = 1$, but in the continuum model we can add particles even when all potential wells are filled. The additional particles will reside in interstitial positions in between the wells. The density is defined as $\rho = N/A$. Thus the coverage $\theta = 1.0$ corresponds to the density $\rho = 0.25$ with the current

(a) Tracer diffusion for $\theta \leq 1$.

(b) Tracer diffusion for higher densities.

Figure 5.3: The tracer diffusion coefficient D_T at the high friction regime $\eta/\omega_0 = 10$. Diamonds are the smooth surface results of Table 5.1, squares for $V_0 = 0.2$, circles for $V_0 = 0.3$. The solid line is the mean field result $D_T(\theta)/D_T(0) = 1 - \theta$ for the Langmuir gas and the dotted line is obtained from Eq. (5.2.2). Other lines are intended as guides to the eye only.

surface potential.

In Fig. 5.3 we can see that as the surface potential amplitude V_0 increases the behavior of the tracer diffusion coefficient indeed approaches that of the Langmuir lattice gas. For $V_0 = 0.3$ the agreement is good up to the coverage of about $\theta \approx 0.7$. The result for the true Langmuir gas model presented for comparison is obtained from the approximate expression by Ferrando *et al.* [18]

$$D_T(\theta)/D_T(0) = (1 - \theta) \left(1 - \frac{2\theta}{6 - \theta - 2\xi + \xi\theta} \right), \quad (5.2.2)$$

where $\xi = 10440/9443$. We find this formula to be in excellent agreement with the MC simulation results by Tahir-Kheli *et al.* [17].

An interesting phenomenon occurs in the continuum model when the number of particles is larger than the number of wells in the system. The tracer diffusion coefficient is seen to shoot up sharply, even above the smooth surface results. This behavior is due to the particles which travel in between the wells never finding an unoccupied well to settle into. The mobility of

5.2 The influence of an external potential

| ρ | $D_T(\rho)/D_T(0)$ | | | Eq. (5.2.2) |
|--------|----------------------|-------------|-----------------------|-------------|
| | $\eta/\omega_0 = 10$ | | $\eta/\omega_0 = 0.1$ | |
| | $V_0 = 0.2$ | $V_0 = 0.3$ | $V_0 = 0.2$ | |
| 0 | 1 | 1 | 1 | 1 |
| 0.0375 | 0.83(4) | 0.81(5) | 0.69(2) | 0.783 |
| 0.0750 | 0.68(3) | 0.62(4) | 0.48(1) | 0.590 |
| 0.1125 | 0.54(2) | 0.46(3) | 0.33(1) | 0.421 |
| 0.1500 | 0.40(2) | 0.32(3) | 0.234(6) | 0.275 |
| 0.1884 | 0.30(1) | 0.22(1) | 0.182(5) | 0.150 |
| 0.2250 | 0.26(1) | 0.14(3) | 0.195(6) | 0.0537 |
| 0.2500 | 0.36(2) | 0.37(2) | 0.315(7) | 0.0000 |
| 0.2875 | 0.79(4) | 2.66(8) | 0.73(2) | |
| 0.3625 | 1.31(7) | 4.9(2) | 1.24(4) | |
| 0.4375 | 1.35(6) | 4.9(2) | 1.24(4) | |
| 0.5125 | 1.13(6) | 3.9(3) | 1.01(4) | |
| 0.5875 | 0.91(5) | 3.3(2) | 0.79(4) | |

Table 5.3: Numerical values of the normalized tracer diffusion coefficient in the surface potential system.

these particles is further enhanced by the fact that the surface potential tends to pull these particles closer to the particles trapped in the wells. The trapped particles kick around the interstitial particles strongly enhancing their mobility. We checked this effect by increasing the lattice parameter a . This leads to an increase in the average distance between the particles and reduces the effect of the repulsive interactions. As a result D_T decreased over 50 % even with a relatively small increase of less than 10 % in the lattice parameter.

The effect of friction on the tracer diffusion coefficient is illustrated in Fig. 5.4 for the case $V_0 = 0.2$. Lowering the friction makes the particles more mobile and enhances the blocking effect. As a result D_T decreases more rapidly as a function of density than in the high friction regime.

The density dependence of the center of mass mobility D_{cm} is presented in Fig. 5.5 and in Table 5.4. It is also seen to approach the behavior of the Langmuir lattice gas model as the surface potential amplitude is increased. The agreement is again good up to the coverage of about $\theta \approx 0.7$. For the same reason as in the case of tracer diffusion also the center of mass mobility is seen to increase sharply as the number of particles exceeds the

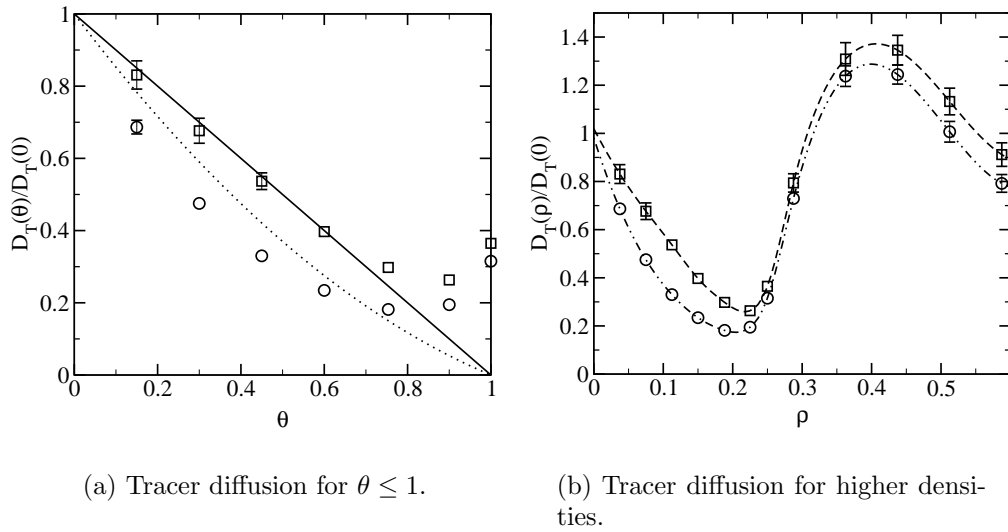


Figure 5.4: The tracer diffusion coefficient D_T at the low friction regime $\eta/\omega_0 = 0.1$. The squares are the high friction data and the circles the low friction data. The lines are as in Fig. 5.3.

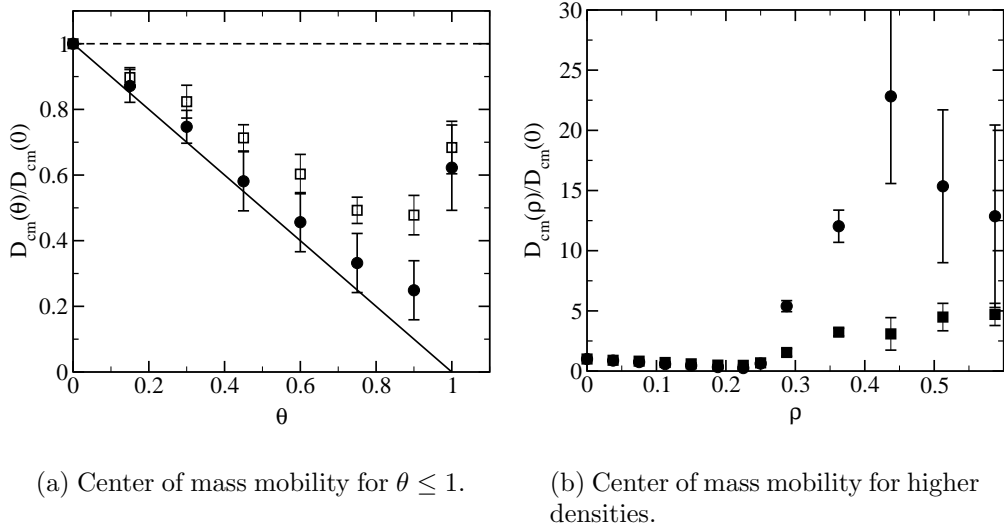


Figure 5.5: The center of mass mobility D_{cm} . The dashed line is the analytic result for the smooth surface case and the solid line is the exact result for the Langmuir gas. Other symbols are as in the previous Figure.

5.2 The influence of an external potential

| ρ | $D_{cm}(\rho)/D_{cm}(0)$ | | ρ | $D_{cm}(\rho)/D_{cm}(0)$ | |
|--------|--------------------------|-------------|--------|--------------------------|-------------|
| | $V_0 = 0.2$ | $V_0 = 0.3$ | | $V_0 = 0.2$ | $V_0 = 0.3$ |
| 0 | 1 | 1 | | | |
| 0.0375 | 0.90(3) | 0.87(5) | 0.2500 | 0.68(8) | 0.6(1) |
| 0.0750 | 0.82(5) | 0.75(5) | 0.2875 | 1.5(3) | 5.4(5) |
| 0.1125 | 0.71(4) | 0.58(9) | 0.3625 | 3.2(3) | 12(1) |
| 0.1500 | 0.60(6) | 0.46(9) | 0.4375 | 3(1) | 23(7) |
| 0.1884 | 0.49(4) | 0.33(9) | 0.5125 | 4(1) | 15(6) |
| 0.2250 | 0.48(6) | 0.25(9) | 0.5875 | 5(1) | 13(7) |

Table 5.4: Numerical values of the normalized center of mass mobility in the surface potential system.

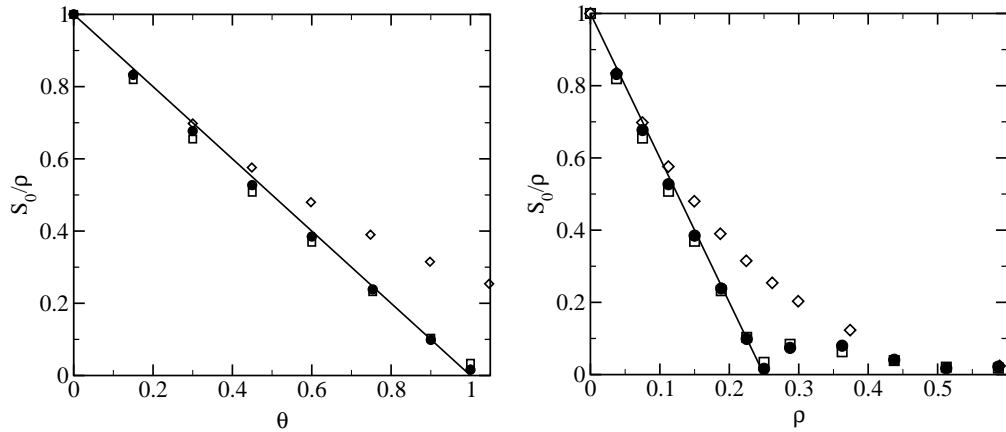
| ρ | S_0/ρ | | ρ | S_0/ρ | |
|--------|-------------|-------------|--------|-------------|-------------|
| | $V_0 = 0.2$ | $V_0 = 0.3$ | | $V_0 = 0.2$ | $V_0 = 0.3$ |
| 0 | 1 | 1 | | | |
| 0.0375 | 0.8192(4) | 0.8325(2) | 0.2500 | 0.034(2) | 0.016(4) |
| 0.0750 | 0.6548(2) | 0.6773(5) | 0.2875 | 0.084(2) | 0.074(9) |
| 0.1125 | 0.5075(4) | 0.5273(7) | 0.3625 | 0.063(3) | 0.080(2) |
| 0.1500 | 0.3690(2) | 0.3848(3) | 0.4375 | 0.0388(6) | 0.0410(6) |
| 0.1884 | 0.2322(2) | 0.2385(2) | 0.5125 | 0.0206(7) | 0.0174(6) |
| 0.2250 | 0.1033(1) | 0.0986(1) | 0.5875 | 0.018(2) | 0.022(3) |

Table 5.5: Numerical values of the thermodynamic factor in the surface potential system.

number of wells in the continuum system.

In Fig. 5.6 and Table 5.5 we show the behavior of the thermodynamic factor S_0/ρ , which is the other component of the collective diffusion coefficient D_C . It is seen that this static quantity agrees extremely well throughout the coverage range with the lattice gas results when the surface potential amplitude is $V_0 = 0.3$. At the highest densities it assumes values very close to the smooth surface results.

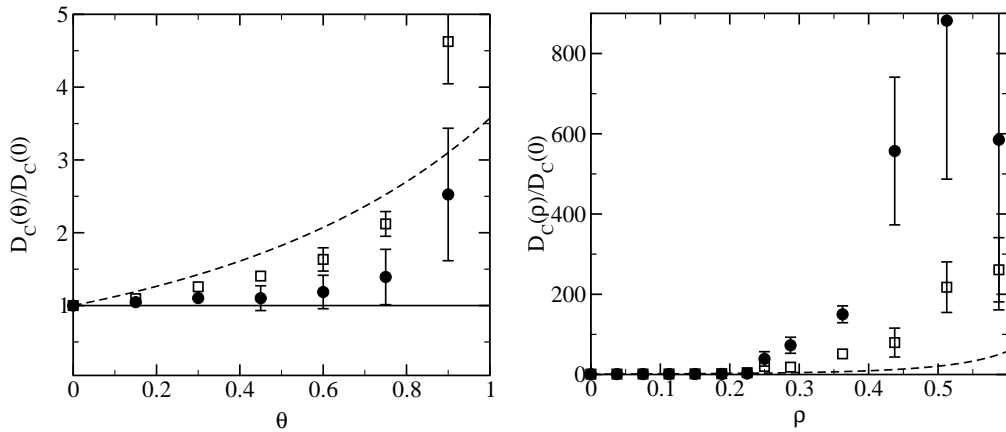
Combining the two factors D_{cm} and ρ/S_0 presented above we get the behavior of the collective diffusion coefficient D_C . This we present in Fig. 5.7. Agreement with the lattice gas model is again very good up to coverages around $\theta \approx 0.7$. Beyond that the rapid increase is due to the increase in the center of mass mobility D_{cm} . In this system the collective diffusion co-



(a) Thermodynamic factor for $\theta \leq 1$.

(b) Thermodynamic factor for higher densities.

Figure 5.6: The thermodynamic factor S_0/ρ . The solid line is the exact analytic result $(1 - \theta)$ for the Langmuir gas, diamonds are smooth surface data, squares for $V_0 = 0.2$, and circles for $V_0 = 0.3$.



(a) Collective diffusion for $\theta \leq 1$.

(b) Collective diffusion for higher densities.

Figure 5.7: The collective diffusion coefficient D_C . The solid line is the exact analytic result $D_C/D_C(0) = 1$ for the Langmuir gas, the dashed line is the smooth surface result. Other symbols are as in Fig. 5.6

5.2 The influence of an external potential

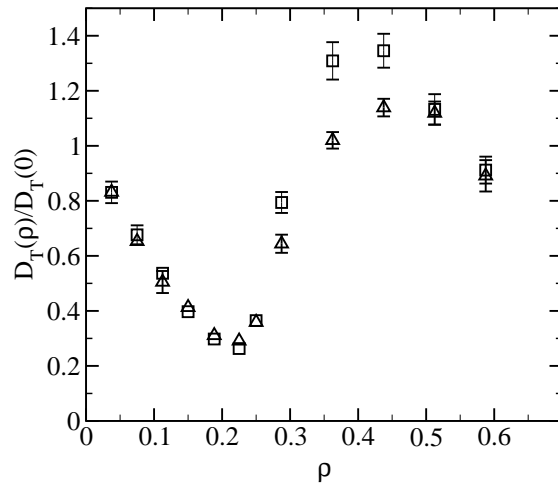


Figure 5.8: The tracer diffusion coefficient in the system with the non-separable surface potential. The squares are the data with the separable surface potential (5.2.1) and the triangles for the non-separable surface potential (5.2.3).

efficient displays a maximum at a density larger than $\theta = 1$ in contrast to the monotonically increasing behavior seen in the smooth surface system. This is due to the decreasing mobility at the highest densities.

We also performed additional simulations using a non-separable surface potential appropriate for a bcc(110) surface symmetry

$$V_A(x, y) = \tilde{V}_0 \left[1 + \sin\left(\frac{2\pi x}{\tilde{a}}\right) \sin\left(\frac{2\pi y}{\sqrt{2}\tilde{a}}\right) \right], \quad (5.2.3)$$

where \tilde{a} is the lattice parameter. We chose \tilde{a} such that the density of the minima in (5.2.3) was the same as with the separable potential (5.2.1) and the amplitude was set to $\tilde{V}_0 = 0.4$ which makes the barrier between the minima match the barrier of the separable potential when $V_0 = 0.2$. The data are presented in Fig. 5.8 and in Table 5.6. At the high friction regime the one-particle diffusion coefficient turned out to be about 25 % lower than in the case of the separable potential but the density dependence of the tracer diffusion coefficient D_T below the coverage $\theta = 1$ was within error bars exactly the same. At higher densities D_T in the non-separable surface potential system was slightly lower.

| $\tilde{\rho}$ | $D_C(\tilde{\rho})/D_C(0)$ | $\tilde{\rho}$ | $D_C(\tilde{\rho})/D_C(0)$ |
|----------------|----------------------------|----------------|----------------------------|
| 0 | 1 | | |
| 0.0375 | 0.83(3) | 0.2500 | 0.36(1) |
| 0.0750 | 0.65(2) | 0.2875 | 0.64(3) |
| 0.1125 | 0.51(4) | 0.3625 | 1.02(3) |
| 0.1500 | 0.41(1) | 0.4375 | 1.14(3) |
| 0.1884 | 0.31(1) | 0.5125 | 1.12(4) |
| 0.2250 | 0.29(1) | 0.5875 | 0.89(6) |

Table 5.6: Numerical values of the normalized tracer diffusion coefficient for the non-separable surface potential system.

5.3 The velocity autocorrelation functions in the surface systems

A quantity of central importance for the tracer diffusion coefficient is the velocity autocorrelation function $\phi(t)$ as explained in Section 2.2. In fact, using Eq. (2.2.6) D_T can be calculated from the velocity autocorrelation function. Recently it has been demonstrated that in many cases $\phi(t)$ displays an intermediate time power law decay $\phi(t) \propto t^{-x}$, where the value of the effective exponent x can be related to interaction and ordering effects in the system [50]. In Publication III we explore the value of this exponent in various systems.

The time dependence of $\phi(t)$ on a smooth surface was studied in Publication II and on the surface with periodic surface potential in Publication IV. However, because of the relatively short power law regime it was difficult to determine x accurately. Also the location of the power law regime can be difficult to pinpoint. Due to these difficulties the values reported in Publication IV were not accurate. For the Langmuir gas there exists an analytic solution for the velocity autocorrelation function [51–53]. In the Langmuir gas system the decay exponent $x \approx 2.0$.

The velocity autocorrelation functions in the surface systems are presented in Fig. 5.9 along with the corresponding memory functions. The exponents x are also indicated in the Figure. The exponents reported in Publication IV were taken from the beginning of the curve shown here. The density in all cases is $\rho = 0.1884$ or $\theta = 0.75$. Based on the Langmuir gas results it is expected that at this density the effect is most pronounced. In the

5.4 Diffusion of rodlike molecules

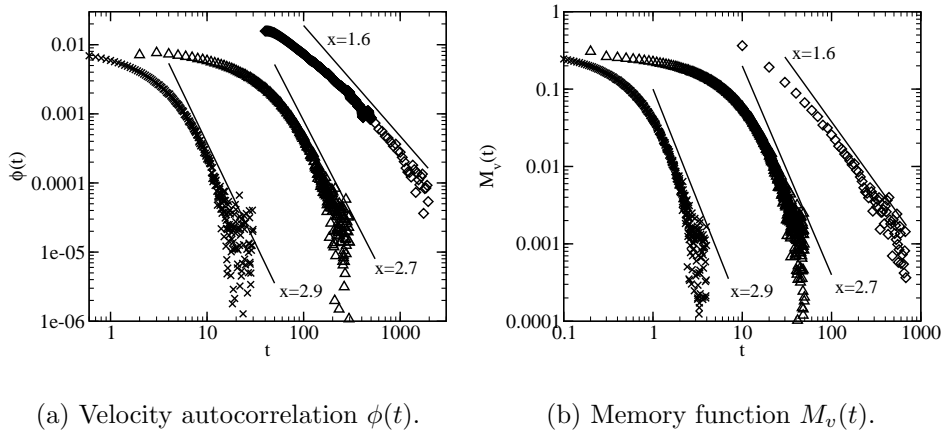


Figure 5.9: The velocity autocorrelation functions and corresponding memory functions in the surface systems. The diamonds are data on a smooth surface, the triangles data for the system with the separable surface potential with amplitude $V_0 = 0.2$ and the crosses for $V_0 = 0.3$. The data have been shifted for clarity.

smooth surface system the exponent $x \approx 1.6$. This value seems to increase slightly with increasing density.

Increasing the surface potential amplitude increases the exponent such that at the system with strongest surface potential $V_0 = 0.3$ the exponent $x \approx 2.9$. This value, which is larger than the Langmuir gas value is in agreement with the result in Publication III that the exponent tends to increase with increasing particle-particle repulsion. The obtained values are also close to the values reported in literature [50, 53, 54].

5.4 Diffusion of rodlike molecules

The system of single spherical particles presented above is, of course, the most simple surface system imaginable. However, the real molecules in nature come in a multitude of shapes and sizes. One still rather simple system is the case of chain-like molecules studied by Hjelt *et al.* [7, 55]. They studied the dynamics of chain-like molecules with several chain lengths and stiffnesses using the fluctuating bond model. In this thesis we study a special

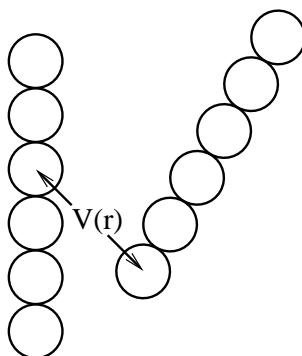


Figure 5.10: A schematic figure of the rodlike molecules used in the simulations.

case of such molecules the infinitely stiff rodlike limit. This work has been presented in Publications I and II.

We model the rodlike molecules by using N_l single spheres which are forced to stay on the same line forming a rod. This is illustrated in Fig. 5.10. Between these spheres we have the same interaction as in the case of single spheres. At every time step we calculate the forces acting on every sphere comprising the rodlike molecule and from them we determine the torque and the force on the center of mass of the molecule. The molecule is then moved and rotated accordingly. There is no surface potential, i.e. the surface is taken to be smooth. We have studied rod lengths of $N_l = 3$, $N_l = 6$ and $N_l = 11$.

The phase diagram of the system is similar to the case of the single spheres except that for the rods there exists the possibility of a nematic phase in which all the rods line up and point in the same direction. However, this phase is not realized for aspect ratios of roughly six and less [56]. The densities studied in the system of rods of length $N_l = 11$ were lower than the density required for a nematic phase. As with the single spheres all the studied rodlike molecule systems were well within the liquid phase. The density is here again defined as $\rho = N/A$ and N is still the number of spheres in the system and there are N_l spheres in each rod. The scaling of the density that was used in the single sphere case to obtain the hard sphere results is not valid for the rodlike molecules and therefore all the results for them are presented as a function of the bare density ρ .

In Publication I we have applied the Boltzmann-Matano method described

5.4 Diffusion of rodlike molecules

| ρ | $D_C(\rho)/D_C(0)$ | | |
|--------|--------------------|-------------|---------|
| | $1/r^{12}$ | hard sphere | Boublik |
| 0 | 1 | 1 | 1 |
| 0.0630 | 1.64(4) | 1.46(2) | 1.470 |
| 0.1254 | 2.83(4) | 2.14(4) | 2.082 |
| 0.1800 | 4.41(6) | 3.00(5) | 2.783 |
| 0.2514 | 8.2(3) | 4.43(7) | 4.035 |
| 0.3144 | 13.3(4) | 6.0(1) | 5.608 |
| 0.4080 | 29(2) | 9.5(5) | 9.314 |
| 0.4950 | 57(4) | 13.5(9) | 15.51 |

Table 5.7: Numerical values of the normalized collective diffusion coefficient in a system of $N_l = 6$ rodlike molecules for two different interaction potentials, the $1/r^{12}$ and the hard sphere potentials. Also shown are values obtained from Boublik's approximation Eq. (2.7.6).

in Section 4.3.2 to determine the collective diffusion coefficient for the rodlike molecules. There was a scaling error in the results published in Publication I such that the molecules did not have the indicated number of molecules in them, but there was an empty site in between all of the spheres. This made the molecules effectively longer than intended such that the aspect ratio of the six particle molecules was actually 11 and the aspect ratio of the dimers was actually 3. However, snapshots of the systems indicated that the particles did not pass through each other or penetrate each other despite these holes.

In Fig. 5.11 we present the collective diffusion coefficient obtained both by the Boltzmann-Matano analysis and equilibrium simulations. The equilibrium data are also tabulated in Table 5.7. In the Figure it is seen that D_C is a strongly increasing function of density and the increasing aspect ratio of the rods further enhances this effect. The data for the $N_l = 11$ rods are presented as if there were really 11 particles in each rods and of course, they are not directly comparable with the six-particle rods because of the slightly different shape of these molecules. We expect the effect of this to be rather small though. The maximum in D_C reported in Publication I is an artifact of the Boltzmann-Matano method and is not really there as our later equilibrium simulations in Publication II have confirmed. Such a maximum at intermediate densities does appear for flexible, chainlike molecules as demonstrated in Refs. [7, 55].

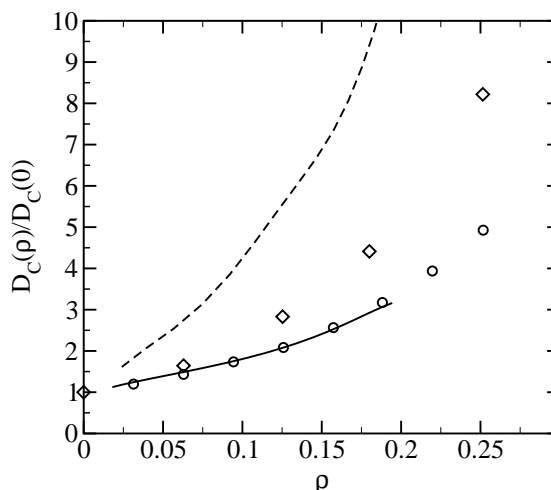


Figure 5.11: The collective diffusion coefficient for the rodlike molecules. The dashed line represents our Boltzmann-Matano simulation data for the rods of effective length $N_l = 11$, the diamonds are the equilibrium simulation data for rods of length $N_l = 6$, the solid line and the circles are comparison data for single particles from Boltzmann-Matano analysis and equilibrium simulations, respectively.

We also tried to estimate the collective diffusion coefficient for the rods using Boublik's approximation Eq. (2.7.6) ignoring the fact that the rods are not completely convex. Since Boublik's approximation only applies to hard particles and the scaling of the density used for single spheres is not applicable to the rods we performed separate simulations with the rods using the true hard sphere potential. The results are presented in Fig. 5.12 and in Table 5.7. For comparison we also present the results for the softer $1/r^{12}$ potential in the same Figure. As in the case of single spheres above, the agreement is very good at the lower densities and the approximation tends to overestimate the results a little at the highest densities.

The tracer diffusion coefficient of a single rod can be obtained from the same equation as D_T for a single particle, i.e. Eq. (2.2.2), only the mass of the rod is N_l times the mass of a single sphere. In Fig. 5.13 and Table 5.8 we present the data for the tracer diffusion coefficient for the rodlike molecules. Interestingly, it matches almost exactly the data of the single spheres. It seems that the additional constraint binding N_l molecules together only affects the absolute value of the diffusion coefficient but not the functional form of its density dependence. It is an interesting question whether this

5.4 Diffusion of rodlike molecules

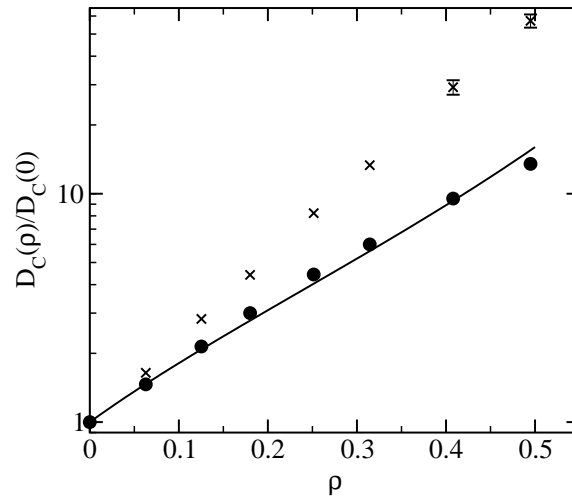


Figure 5.12: The collective diffusion for hard rods (circles). For comparison the crosses represent the same data using the softer $1/r^{12}$ potential. The solid line is the Boublik approximation Eq. (2.7.6).

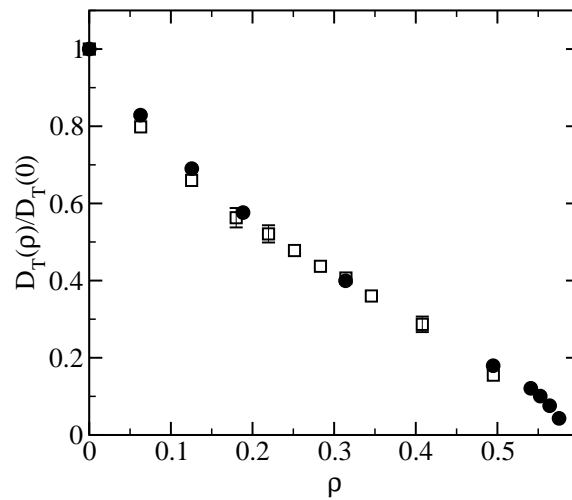


Figure 5.13: The tracer diffusion coefficient for the rodlike molecules. The squares are the simulation data for the rods of length $N_l = 6$ and the circles are the corresponding data for single particles.

| ρ | $\frac{D_T(\rho)}{D_T(0)}$ | $\frac{D_R(\rho)}{D_R(0)}$ | ρ | $\frac{D_T(\rho)}{D_T(0)}$ | $\frac{D_R(\rho)}{D_R(0)}$ |
|--------|----------------------------|----------------------------|--------|----------------------------|----------------------------|
| 0 | 1 | 1 | | | |
| 0.0630 | 0.80(1) | 0.88(5) | 0.2832 | 0.44(1) | 0.36(2) |
| 0.1254 | 0.66(2) | 0.79(5) | 0.3144 | 0.41(1) | 0.29(3) |
| 0.1800 | 0.56(3) | 0.64(3) | 0.3456 | 0.36(1) | 0.23(1) |
| 0.2196 | 0.52(2) | 0.50(3) | 0.4080 | 0.29(2) | 0.15(1) |
| 0.2514 | 0.48(1) | 0.46(2) | 0.4950 | 0.16(1) | 0.049(6) |

Table 5.8: Numerical values of the normalized tracer diffusion coefficient and angular diffusion coefficient in a system of $N_l = 6$ rodlike molecules.

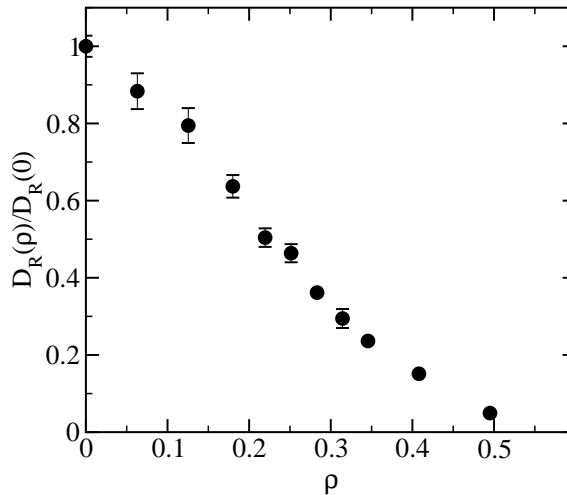


Figure 5.14: The angular diffusion coefficient for the rodlike molecules of length $N_l = 6$.

is valid for molecules of any shape. Based on our results it would seem so, but since we have only studied rodlike molecules with one aspect ratio we cannot answer the question conclusively.

For the purpose of monitoring the orientational ordering we also computed the behavior of the angular diffusion coefficient D_R defined by Eq. (2.4.1). The results are presented in Fig. 5.14 and in Table 5.8. No sharp drop in the data can be seen which would indicate that there is no transition to a nematic phase in this system in agreement with results of Bates and Frenkel [56].

5.5 Sedimentation of non-colloidal particles

5.5.1 Three dimensional system

The sedimentation of non-colloidal particles is an interesting example of non-equilibrium dynamics. It displays Brownian dynamics like behavior in a completely deterministic system. When a single particle falls in a liquid it follows a straight line and reaches a terminal velocity given by Eq. (3.1.8). When there are more particles in the system the trajectories of the particles become chaotic because of the hydrodynamic interactions between the particles. Even the average sedimentation velocity becomes a non-trivial matter.

In this thesis we study sedimentation in a system of spherical particles and in a system of prolate spheroids of aspect ratios a_r of 3, 5, and 7. The aspect ratio of a spheroid is defined as half of the length of the axis of symmetry divided by the largest radius perpendicular to the axis. The radius of the spherical particles was set to unity. The density of the particles was chosen to be 2.5 times the density of the fluid. The fluid viscosity was fixed such that the Reynolds number was $0.5a_r$. The simulations were carried out in the regime of a large Péclet number ($Pe^{-1} = 0$), that is Brownian motion plays no role in the dynamics.

In Fig. 5.15 we show the average sedimentation velocity in a system of spherical particles and in a system of spheroids as a function of the particle volume fraction Φ in a three dimensional system. The system size was $32 \times 32 \times 64$ in units of the smaller radius of the particles the largest dimension being parallel to gravity. We have periodic boundary conditions in all directions. We see that all systems follow the Richardson-Zaki law (3.1.9) at high volume fractions. At low volume fractions the sedimentation velocity of the spherical particles decreases more rapidly than in the RZ-picture. This is in agreement with experiments [57]. The most striking feature seen in Fig. 5.15, however, is that the sedimentation velocity of the spheroids not only deviates from the RZ-law but it behaves non-monotonically and displays a maximum at an intermediate volume fraction. This behavior has also been seen experimentally [58, 59].

The above described behavior suggests that the settling velocity of the spheroid system is affected by the orientational ordering of the particles. In Publication V we have confirmed this by examining the orientational

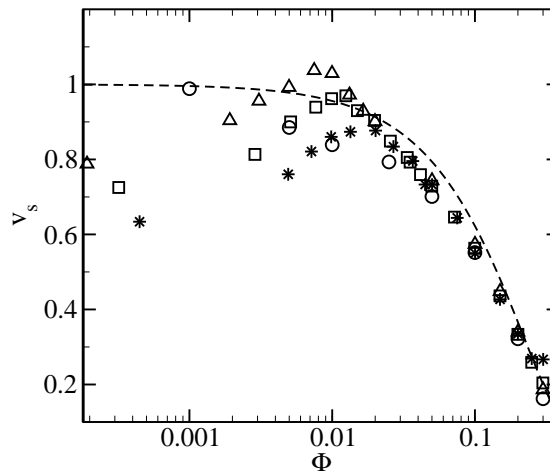


Figure 5.15: The average sedimentation velocity as a function of the volume fraction in systems of spheroids of different aspect ratios a_r . The circles represent data with $a_r = 1$ (the spheres), the triangles $a_r = 3$, the squares $a_r = 5$, and the stars $a_r = 7$. The dotted line is the Richardson-Zaki law $(1 - \Phi)^{4.5}$.

distribution and an order parameter $\psi = \langle 2 \cos \theta - 1 \rangle$ as a function of the volume fraction Φ of the particles. Here θ denotes the angle between the axis of symmetry of the spheroid and gravity. In Fig. 5.16 we show the orientational distribution of the spheroids with different volume fractions. It can be seen that in the most dilute systems the spheroids are mostly oriented perpendicular to gravity. This is the orientation that a single isolated spheroid would prefer. However, as the volume fraction is increased, more and more particles are oriented parallel to the gravity. The maximum of the average sedimentation velocity occurs roughly at the same volume fraction where the orientation distribution is seen to be flat.

The change in the orientational distribution can be quantified by computing the order parameter ψ . The value of ψ varies from -1 to 0 to +1 if all the spheroids were perpendicular to gravity, randomly oriented, or parallel to gravity, respectively. We show the behavior of this order parameter as a function of the volume fraction Φ in Fig. 5.17. The values of Φ where $\psi \approx 0$ corresponds roughly to the maximum of the average sedimentation velocity. Also the susceptibility of the order parameter shown in the inset displays a broad maximum reflecting the existence of an orientational transition region.

5.5 Sedimentation of non-colloidal particles

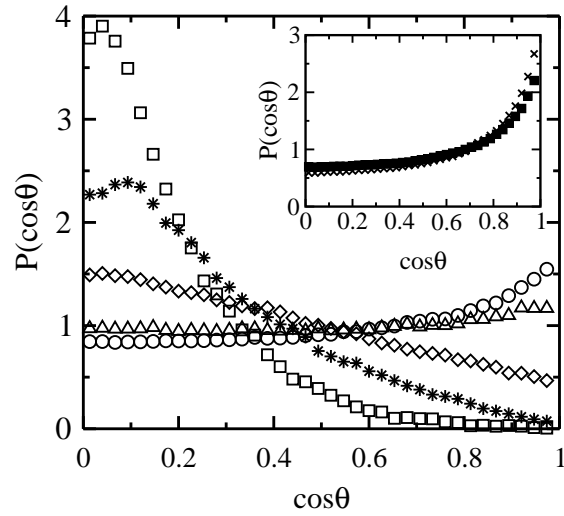


Figure 5.16: The orientation distribution function $P(\cos\theta)$ for spheroids of aspect ratio $a_r = 5$ at different volume fractions Φ . Open squares denote data with $\Phi = 0.0029$, stars $\Phi = 0.005$, diamonds $\Phi = 0.0099$, triangles $\Phi = 0.019$, and circles $\Phi = 0.034$. The inset shows the volume fractions $\Phi = 0.1$ as solid squares and $\Phi = 0.20$ as crosses.

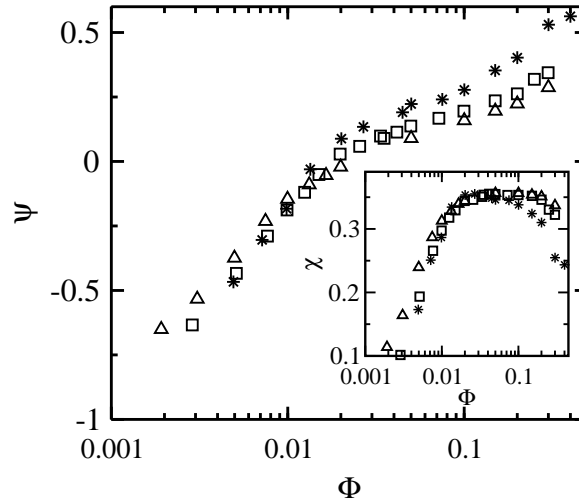


Figure 5.17: The order parameter $\psi = \langle 2 \cos\theta - 1 \rangle$ for spheroids of different aspect ratios a_r as a function of the volume fraction Φ . The aspect ratios are $a_r = 3$ (triangles), $a_r = 5$ (squares), and $a_r = 7$ (stars). The inset shows the susceptibility $\chi = \langle \psi^2 \rangle - \langle \psi \rangle^2$ of the order parameter.

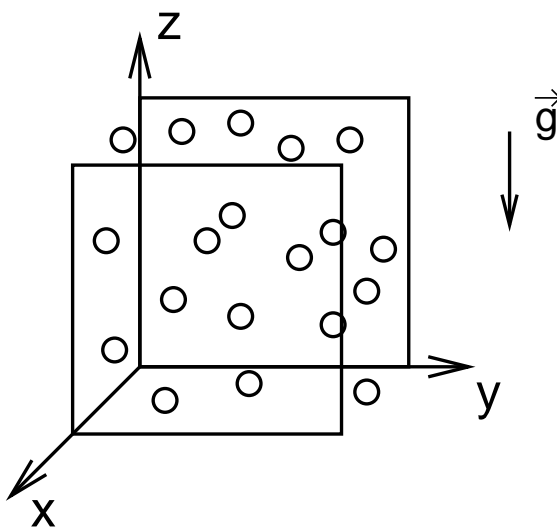


Figure 5.18: The sedimenting system between two parallel vertical walls.

5.5.2 System confined between walls

We also studied a system of spherical particles confined between two vertical walls [1]. The system is illustrated schematically in Fig. 5.18. The wall spacing L_x was varied from 3.2 particle radii to 45.87 particle radii. The other dimensions of the system were 22.76 particle radii with periodic boundary conditions. Gravity points to the negative z direction. The thinnest system is quasi-2D since the particles cannot pass each other in the direction of the walls and the behavior of the widest system is close to the 3D system.

In Fig. 5.19 we show the average sedimentation velocity. It is seen to obey well the phenomenological Richardson-Zaki law (3.1.9). The curves in the Figure are fits of the Richardson-Zaki law to the data and it is observed that the Richardson-Zaki exponent n_{RZ} changes from the quasi two dimensional value of 3.5 towards the value 5.5, which is close to what has been observed in three dimensional systems [60].

As was explained in Section 3.1 an interesting unsettled question concerns the velocity fluctuations in a sedimenting system. In Figures 5.20, 5.21 and 5.22 we present the observed velocity fluctuations in this system in x , y , and z directions, respectively. The general behavior as a function of volume fraction Φ is the same in all directions. In the beginning there is an increasing part which is easy to understand as for a single particle the sedimentation velocity is constant and there are no fluctuations. When the

5.5 Sedimentation of non-colloidal particles

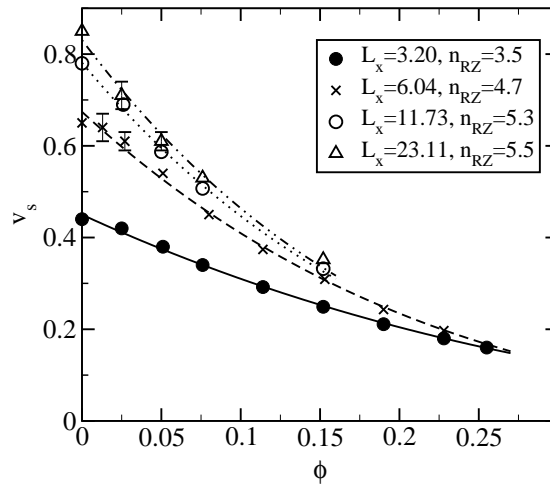


Figure 5.19: The average sedimentation velocity in the system confined between two vertical walls. The lines are fits to the Richardson-Zaki law (3.1.9) with exponents n_{RZ} indicated in the legend.

volume fraction increases the particles interact more and more and produce larger velocity fluctuations. However, beyond some volume fraction there are so many particles in the system that they start blocking the motion of each other and the velocity fluctuations start decreasing. This decrease is seen to be roughly linear, which has also been seen experimentally [61].

However, the most interesting question concerns the magnitude of the velocity fluctuations as a function of the system size. In Figs. 5.20 and 5.21 it is seen that the horizontal velocity fluctuations saturate. In the x direction perpendicular to the walls the walls restrict the motion especially at the smallest systems and the saturation is slower. As the system width is increased also the fluctuations in the x direction eventually saturate to the same value as in the y direction.

In the z direction parallel to gravity we see that in the quasi-2D system the velocity fluctuations are roughly the same as in the horizontal y direction. This is in agreement with experiments performed in a fluidized bed system [62]. However, in the y direction the fluctuations do not saturate but grow as the cube root of the width of the system as illustrated in Fig. 5.22 (b). This is exactly what is expected from simple theoretical arguments explained in Section 3.1 and no screening mechanism which would suppress them seems to be emerging for the system sizes studied.

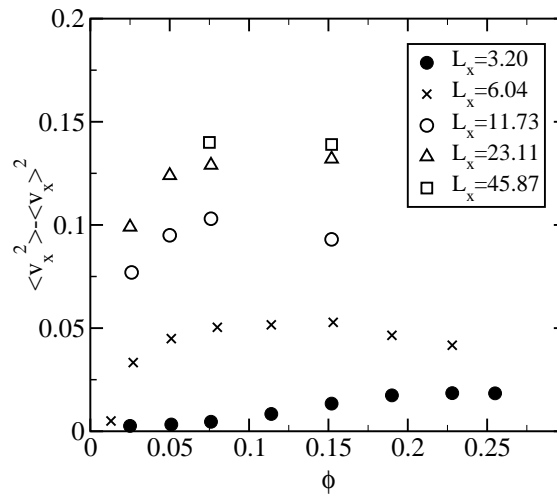


Figure 5.20: The velocity fluctuations in the x direction perpendicular to the walls.

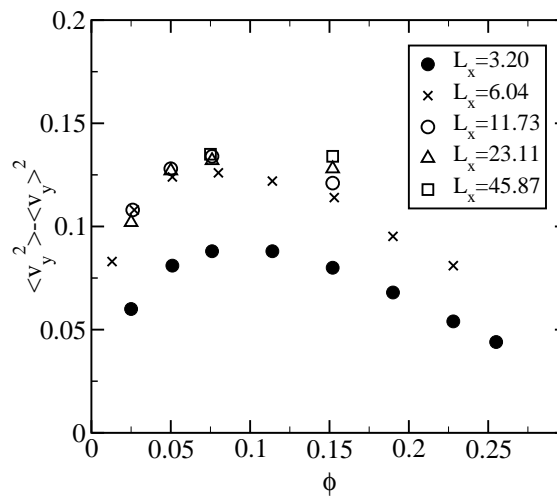


Figure 5.21: The velocity fluctuations in the horizontal y direction parallel to the walls.

5.6 Velocity autocorrelation function in the sedimentation system

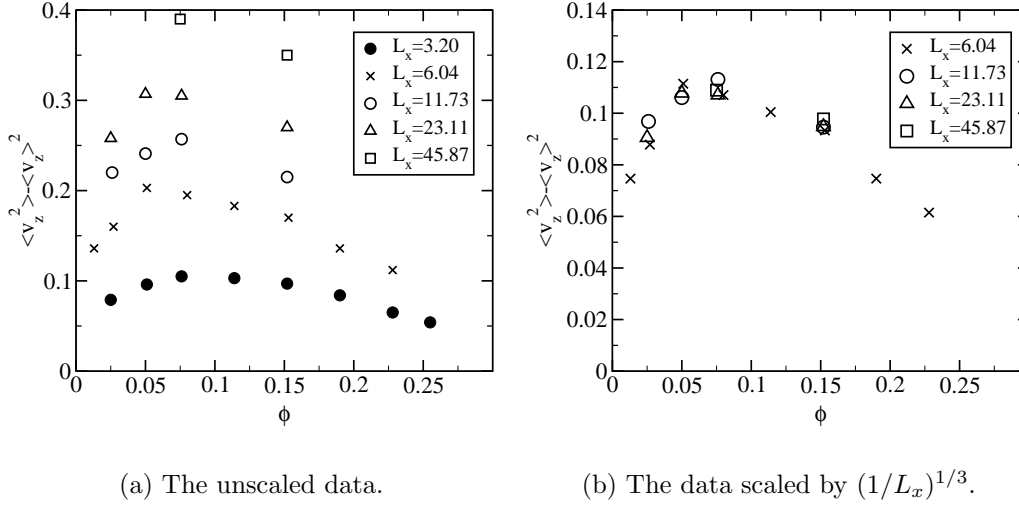


Figure 5.22: The velocity fluctuations in the z direction parallel to gravity.

We also studied the behavior of the tracer diffusion coefficient defined in Section 3.1 by Eq. (3.1.11). The tracer diffusion coefficient as a function of the volume fraction Φ is presented in Figs. 5.23 and 5.24 in y and z directions, respectively. The same monotonically decreasing behavior as seen in the Brownian surface systems can also be seen here in most cases. The maximum seen in some of the systems in the horizontal direction is due to the increasing velocity fluctuations in the low volume fractions as shown above. In the direction parallel to gravity the tracer diffusion coefficient can be seen to saturate as a function of increasing system size. This is again due to the similar behavior displayed by the corresponding velocity fluctuations.

5.6 Velocity autocorrelation function in the sedimentation system

We also evaluated the decay exponent of the velocity fluctuation autocorrelation function $C_\alpha(t)$ in the sedimentation system. The only clear evidence of a presence of algebraic decay in $C_\alpha(t)$ was seen in the quasi-2D system in the direction parallel to gravity. We present $C_z(t)$ in that system in Fig. 5.25. The values of the decay exponent x are indicated in the Figure

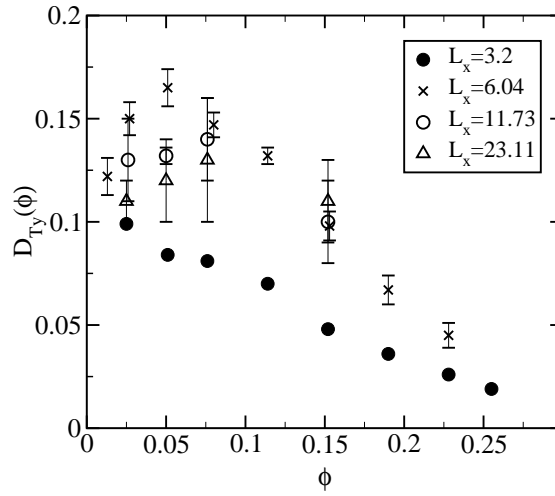


Figure 5.23: The tracer diffusion coefficient in the horizontal y direction parallel to the walls.

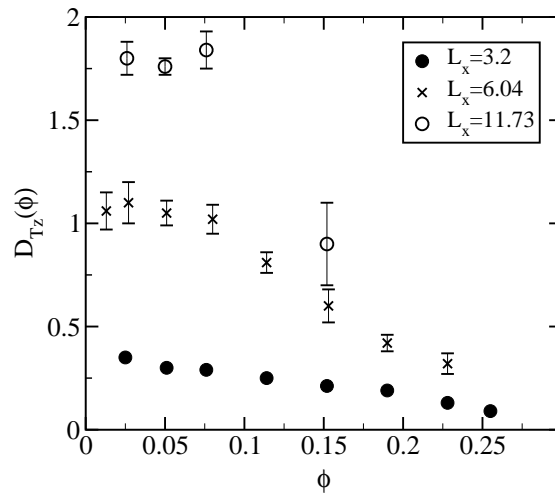
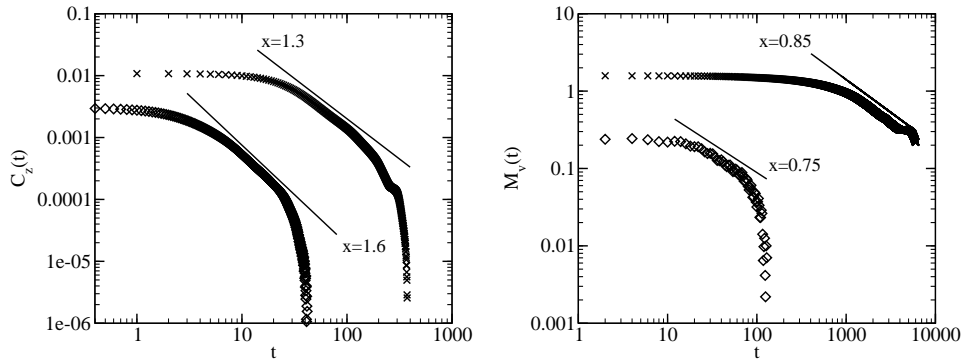


Figure 5.24: The tracer diffusion coefficient in the z direction parallel to gravity.

5.6 Velocity autocorrelation function in the sedimentation system



(a) Velocity fluctuation autocorrelation $C_z(t)$.

(b) Memory function $M_v(t)$.

Figure 5.25: The velocity fluctuation autocorrelation functions and corresponding memory functions in the sedimentation systems. The diamonds are data for a volume fraction $\Phi = 0.255$ and the crosses for $\Phi = 0.076$. The data have been shifted for clarity.

and they are of the same order of magnitude as the corresponding exponents observed in the surface systems. When the spacing between the walls confining the system was increased this behavior vanished and was not observed in the 3D system.

Chapter 6

Summary and discussion

In this thesis we have studied the diffusive dynamics of interacting many-particle systems through extensive computer simulations. The central quantities used for describing this are the diffusion coefficients, namely the tracer and collective diffusion coefficients D_T and D_C , respectively, and the correlation functions associated with them.

This many-body problem is in general impossible to solve analytically and theoretical understanding of it is far from complete. Computer simulations offer a well controlled way of studying such systems and obtaining information about their behavior.

Towards this end we have studied the behavior of several different systems. First we looked at the case of Brownian dynamics on surfaces. The most simple such system is the hard sphere system on a smooth surface. In this system the tracer diffusion coefficient was found to be a monotonously decreasing function of density. The collective diffusion coefficient, on the other hand, was found to be a monotonously increasing function of density due to the behavior of the isothermal compressibility.

Then we went on to consider the effect of a periodic surface potential on the dynamics. A system with a surface potential was compared with the simple and widely used lattice gas system. The behavior of the continuum system with a periodic surface potential was found to agree well with the lattice gas model in the high friction regime provided that the surface potential amplitude was strong enough.

As an example of slightly more complicated molecules we considered a system of stiff rodlike molecules. We showed that the behavior of the normal-

ized tracer diffusion coefficient in this system is essentially the same as that of the single spheres. The increase of the collective diffusion coefficient as a function of density, on the other hand, was seen to be strongly enhanced by the entropic repulsion of the rods.

Finally we turned our attention to the non-Brownian system of sedimentation, which nevertheless displays diffusive dynamics. Our treatment of this problem differs from most others in the respect that we have a liquid with a finite Reynolds number and use the full Navier-Stokes equation to describe the motion of the fluid. In the system of sedimenting spheroids we observed non-monotonic behavior in the average sedimentation velocity, which was attributed to a change in the orientational distribution of the particles.

Within the non-equilibrium sedimentation system we can use the generalized velocity fluctuation autocorrelation function to define the diffusion coefficients. The behavior of the such defined tracer diffusion coefficient was determined in a system confined between two vertical walls, the wall separation varying from a quasi two dimensional conditions to an almost fully three dimensional system. In addition we also studied the system size dependence of the velocity fluctuations, the nature of which has been under great interest recently. We found that in our system the velocity fluctuations parallel to gravity grow with the increasing system size, whereas the horizontal velocity fluctuations saturate. The same behavior could also be seen in the related tracer diffusion coefficients.

Of all the possible diffusive many-particle systems we have only considered a few examples. Many interesting problems in surface diffusion still remain. For example a lot remains to be done to get quantitative estimates of the behavior of the quantities considered in this thesis under more realistic conditions. However, new simulation methods are emerging and for example in the field of hydrodynamics the method recently proposed by Malevanets *et al.* [63] looks promising. We are already taking steps towards applying this method to study diffusion in a two dimensional colloidal system thus bringing the hydrodynamics in to our models of surface diffusion.

Bibliography

- [1] J. M. Lahtinen, E. Kuusela, and T. Ala-Nissila, unpublished (2002).
- [2] T. Ala-Nissila, R. Ferrando, and S. C. Ying, *Collective and single particle diffusion on surfaces*, Adv. Phys. **51**, 949 (2002).
- [3] R. Gomer, *Diffusion of adsorbates on metal surfaces*, Rep. Prog. Phys. **53**, 917 (1990).
- [4] T. Ala-Nissila and S. C. Ying, *Theory of classical surface diffusion*, Prog. Surf. Sci. **39**, 227 (1992).
- [5] R. Kubo, *The fluctuation-dissipation theorem*, Rep. Prog. Phys. **29**, 255 (1966).
- [6] J.-P. Hansen and I. R. McDonald, *Theory of simple liquids* (Academic Press, London, 1991).
- [7] T. Hjelt, S. Herminghaus, T. Ala-Nissila, and S. C. Ying, *Dynamics of chainlike molecules on surfaces*, Phys. Rev. E **57**, 1864 (1998).
- [8] M. Doi and S. F. Edwards, *The Theory of Polymer Dynamics* (Oxford University Press, Oxford, 1986).
- [9] G. Wahnström, *Diffusion of an adsorbed particle: theory and numerical results*, Surf. Sci. **159**, 311 (1985).
- [10] G. Wahnström, *Diffusion of an adsorbed particle: Dependence on the adatom-substrate interaction*, Phys. Rev. B **33**, 1020 (1986).
- [11] G. Wahnström, *Diffusion of an adsorbed particle: Temperature dependence*, J. Chem. Phys. **84**, 5931 (1986).

- [12] J. P. Boon and S. Yip, *Molecular Hydrodynamics* (Dover, New York, 1980).
- [13] L. Y. Chen and S. C. Ying, *Dynamics of adatoms on solid surfaces*, Phys. Rev. B **49**, 13838 (1994).
- [14] T. Ala-Nissila and S. C. Ying, *Univeral properties of classical surface diffusion*, Phys. Rev. Lett. **65**, 879 (1990).
- [15] R. Kutner, *Chemical diffusion in the lattice gas of non-interacting particles*, Phys. Lett. **81A**, 239 (1981).
- [16] R. A. Tahir-Kheli and R. J. Elliott, *Correlated random walk in lattices: Tracer diffusion at general concentration*, Phys. Rev. B **27**, 844 (1983).
- [17] R. A. Tahir-Kheli and N. El-Meshad, *Correlated diffusion in two-dimensional systems*, Phys. Rev. B **32**, 6166 (1985).
- [18] R. Ferrando and E. Scalas, *Self-diffusion in a 2d lattice gas with lateral interactions*, Surf. Sci. **281**, 178 (1993).
- [19] K. Binder, ed., *Applications of the Monte Carlo Method in Statistical Physics* (Springer-Verlag, New York, 1987).
- [20] J. W. Haus and K. W. Kehr, *Diffusion in regular and disordered lattices*, Physics Reports-Review Section of Physics Letters **150**, 263 (1987).
- [21] A. Danani, R. Ferrando, E. Scalas, and M. Torri, *Lattice-gas theory of collective diffusion in adsorbed layers*, Int. J. Mod. Phys. B **11**, 2217 (1997).
- [22] T. Boublik, *Two-dimensional convex particle liquid*, Mol. Phys. **29**, 421 (1975).
- [23] J. F. Richardson and W. N. Zaki, *Sedimentation and fluidization: I*, Trans. Inst. Chem. Eng. **32**, 35 (1954).
- [24] S. Ramaswamy, *Issues in the statistical mechanics of steady sedimentation*, Adv. Phys. **50**, 197 (2001).
- [25] J. Feng, H. H. Hu, and D. D. Joseph, *Direct simulation of initial value problems for the motion of solid bodies in a newtonian fluid, part 1. sedimentation*, J. Fluid Mech. **261**, 95 (1994).

BIBLIOGRAPHY

- [26] A. J. C. Ladd, *Numerical simulations of particulate suspensions via a discretized boltzmann equation part i. theoretical foundation*, J. Fluid. Mech. **271**, 285 (1994).
- [27] R. Verberg and A. J. C. Ladd, *Lattice-boltzmann model with sub-grid-scale boundary conditions*, Phys. Rev. Lett. **84**, 2148 (2000).
- [28] J. F. Brady and G. Bossis, *Stokesian dynamics*, Ann. Rev. Fluid Mech. **20**, 111 (1988).
- [29] B. Cichocki, B. U. Felderhof, K. Hinsén, E. Wajnryb, and J. Blawdziewicz, *Friction and mobility of many spheres in stokes flow*, J. Chem. Phys. **100**, 3780 (1994).
- [30] K. Höfler and S. Schwarzer, *Navier-stokes simulation with constraint forces: Finite-difference method for particle-laden flows and complex geometries*, Phys. Rev. E **61**, 7146 (2000).
- [31] M. P. Allen and D. J. Tildesley, *Computer Simulation of Liquids* (Oxford University Press, Oxford, 1993).
- [32] F. James, *A review of pseudorandom number generators*, Comput. Phys. Commun. **60**, 329 (1990).
- [33] G. Marsaglia, A. Zaman, and W. W. Tsang, *Toward a universal random number generator*, Stat. Prob. Lett. **8**, 35 (1990).
- [34] A. D. Sokal, *Monte Carlo Methods for the Self-Avoiding Walk*, pp. 47–124, in Binder [64] (1995).
- [35] N. Metropolis, A. W. Rosenbluth, M. N. Rosenbluth, A. H. Teller, and E. Teller, *Equation of state calculations by fast computing machines*, J. Chem. Phys. **21**, 1087 (1953).
- [36] K. Binder and D. W. Heermann, *Monte Carlo Simulation in Statistical Physics* (Springer-Verlag, Berlin, 1988).
- [37] S. C. Ying, I. Vattulainen, J. Merikoski, T. Hjelt, and T. Ala-Nissila, *Memory expansion for diffusion coefficients*, Phys. Rev. B **58**, 2170 (1998).
- [38] C. Matano, *On the relation between the diffusion-coefficients and concentrations of solid metals (the nickel-copper system)*, Jap. J. Phys. **8**, 109 (1933).

- [39] P. Nikunen, I. Vattulainen, and T. Ala-Nissila, *Non-equilibrium effects in profile evolution measurements of surface diffusion*, Surf. Sci. Lett. **447**, L162 (2000).
- [40] H. Weber, D. Marx, and K. Binder, *Melting transition in two dimensions: A finite-size scaling analysis of bond-orientational order in hard disks*, Phys. Rev. B **51**, 14636 (1995).
- [41] H. Löwen, *Dynamical criterion for two-dimensional freezing*, Phys. Rev. E **53**, R29 (1996).
- [42] J. M. Kosterlitz and D. J. Thouless, J. Phys. C **6**, 1181 (1973), J. M. Kosterlitz, J. Phys. C **7**, 1046 (1974), B. I. Halperin and D. R. Nelson, Phys. Rev. Lett. **41**, 121 (1978), A. P. Young, Phys. Rev. B **19**, 1855 (1979).
- [43] A. Jaster, *Computer simulations of the two-dimensional melting transition using hard disks*, Phys. Rev. E **59**, 2594 (1999).
- [44] K. Bagchi, H. C. Andersen, and W. Swope, *Computer simulation study of the melting transition in two dimensions*, Phys. Rev. Lett. **76**, 255 (1996).
- [45] K. Bagchi, H. C. Andersen, and W. Swope, *Observation of a two-stage melting transition in two dimensions*, Phys. Rev. E **53**, 3794 (1996).
- [46] H. Löwen and G. Szamel, *Long-time self-diffusion coefficient in colloidal suspensions: theory versus simulation*, J. Phys.: Condens. Matter **5**, 2295 (1993).
- [47] A. V. Indrani and S. Ramaswamy, *Universal self-diffusion and subdiffusion in colloids at freezing*, Phys. Rev. Lett. **73**, 360 (1994), M. Fuchs, Phys. Rev. Lett. **74**, 1490 (1995), A. V. Indrani and S. Ramaswamy, Phys. Rev. Lett. **74**, 1491 (1995).
- [48] M. Fuchs, *Comment on "universal self-diffusion and subdiffusion in colloids at freezing"*, Phys. Rev. Lett. **74**, 1490 (1995).
- [49] E. J. J. van Rensburg, *Virial coefficients for hard discs and hard spheres*, J. Phys. A: Math. Gen. **26**, 4805 (1993).

BIBLIOGRAPHY

- [50] I. Vattulainen, T. Hjelt, T. Ala-Nissila, and S. C. Ying, *Nonexponential decay of velocity correlations in surface diffusion: The role of interactions and ordering*, J. Chem. Phys. **113**, 10284 (2000).
- [51] D. K. Chaturvedi, *Tracer diffusion in cubic lattices*, Phys. Rev. B **28**, 6868 (1983).
- [52] D. K. Chaturvedi, *Exact solution of continued fraction for tracer diffusion in solids*, J. Phys. C: Solid State Phys. **17**, L449 (1984).
- [53] T. Hjelt, I. Vattulainen, T. Ala-Nissila, and S. C. Ying, *Velocity correlations and memory functions in surface diffusion*, Surf. Sci. **449**, L255 (2000).
- [54] P. B. S. Kumar and M. Rao, *Novel monte carlo approach to the dynamics of fluids: Single-particle diffusion, correlation functions, and phase ordering of binary fluids*, Phys. Rev. Lett. **77**, 1067 (1996).
- [55] T. Ala-Nissila, S. Herminghaus, T. Hjelt, and P. Leiderer, *Diffusive spreading of chainlike molecules on surfaces*, Phys. Rev. Lett. **76**, 4003 (1996).
- [56] M. A. Bates and D. Frenkel, *Phase behavior of two-dimensional hard rod fluids*, J. Chem. Phys. **112**, 10034 (2000).
- [57] E. Barnea and J. Mizrahi, *A generalized approach to the fluid dynamics of particulate systems. part 1. general correlation for fluidization and sedimentation in solid multiparticle systems*, Chem. Eng. J. **5**, 171 (1973).
- [58] B. Herzhaft, E. Guazzelli, M. B. Mackaplow, and E. S. G. Shaqfeh, *Experimental investigation of the sedimentation of a dilute fiber suspension*, Phys. Rev. Lett. **77**, 290 (1996).
- [59] B. Herzhaft and E. Guazzelli, *Experimental study of the sedimentation of dilute and semi-dilute suspensions of fibers*, J. Fluid Mech. **384**, 133 (1999).
- [60] H. Nicolai, B. Herzhaft, E. J. Hinch, L. Oger, and E. Guazzelli, *Particle velocity fluctuations and hydrodynamic self-diffusion of sedimenting non-brownian spheres*, Phys. Fluids **7**, 12 (1995).

BIBLIOGRAPHY

- [61] J.-Z. Xue, E. Herbolzheimer, M. A. Rutgers, W. B. Russel, and P. M. Chaikin, *Diffusion, dispersion, and settling of hard spheres*, Phys. Rev. Lett. **69**, 1715 (1992).
- [62] F. Rouyer, J. Martin, and D. Salin, *Non-gaussian dynamics in quasi-2D noncolloidal suspensions*, Phys. Rev. Lett. **83**, 1058 (1999).
- [63] A. Malevanets and R. Kapral, *Mesoscopic model for solvent dynamics*, J. Chem. Phys. **110**, 8605 (1999).
- [64] K. Binder, ed., *Monte Carlo and Molecular Dynamics Simulations in Polymer Science* (Oxford University Press, Oxford, 1995).